Deliverable No. 9.2

A Model and Data Visualization Toolkit

Grant Agreement No.:	600841
Deliverable No.:	D9.2
Deliverable Name:	A Model and Visualization Toolkit
Contractual Submission Date:	28/02/2017
Actual Submission Date:	28/02/2017

Dissemination Level		
PU	Public	**X**
PP	Restricted to other programme participants (including the Commission Services)	
RE	Restricted to a group specified by the consortium (including the Commission Services)	
CO	Confidential, only for members of the consortium (including the Commission Services)	

COVER AND CONTROL PAGE OF DOCUMENT	
Project Acronym:	**CHIC**
Project Full Name:	Computational Horizons In Cancer (CHIC): Developing Meta- and Hyper-Multiscale Models and Repositories for In Silico Oncology
Deliverable No.:	D9.2
Document name:	CHIC_600841_D9.2_A_Model_And_Visualization_Toolkit_v1
Nature (R, P, D, O)[1]	R
Dissemination Level (PU, PP, RE, CO)[2]	RE
Version:	1
Actual Submission Date:	28.2.2017
Editor: Institution: E-Mail:	Beds

ABSTRACT:

This deliverable 9.2 – **A Model and Visualization Toolkit** – consists of three parts.

The first is a visualization tool called CCGVis. CCGVis is a desktop tool for visualizing and comparing tumours and simulations. CCGVis can import, register and visualize medical data, segmentation data and simulations. It can import various medical formats and CHIC simulations. Images can be imported singly, in image/segmentation pairs, or as time series. Metadata containing information about the segmentation labelling and the image projection can be added in the form of json files. Visualizations include slice and orthoslice views in 2D and 3D, isosurfaces in 3D, volume rendering, comparisons between real and simulated tumours, and plots of tumour growth. An evaluation is presented, showing that CCGVis works well, can be used easily by both medical experts and novices, and is considered a useful tool for viewing data and simulations.

The second part is an image segmentation algorithm for nephroblastoma. The method is a semi-automated technique that includes the interaction of a human expert to perform the extraction of the tumour tissues from MRI images. Results from 24 patients confirmed effective agreement with expert annotations of the tumour tissues.

The third part is a timeline visualization of a medical database. This presents the database as items along a multiscale timeline, which can be zoomed from scales of hours to years. The items are coloured by type and feature metadata in the form of text and thumbnail images. Clustering of items avoids clutter.

[1] **R**=Report, **P**=Prototype, **D**=Demonstrator, **O**=Other

[2] **PU**=Public, **PP**=Restricted to other programme participants (including the Commission Services), **RE**=Restricted to a group specified by the consortium (including the Commission Services), **CO**=Confidential, only for members of the consortium (including the Commission Services)

KEYWORD LIST:

Medical visualization, Computer graphics, Simulation, Tumour, Non small cell lung cancer, Glioblastoma, Nephroblastoma, Wilms' tumour, Image analysis, Segmentation, Database visualization.

The research leading to these results has received funding from the European Community's Seventh Framework Programme (FP7/2007-2013) under grant agreement n^{o} 600841.

The author is solely responsible for its content, it does not represent the opinion of the European Community and the Community is not responsible for any use that might be made of data appearing therein.

MODIFICATION CONTROL			
Version	**Date**	**Status**	**Author**

List of contributors

- Feng Dong, BED
- Nigel McFarlane, BED
- Djibril Kaba, BED

Contents

1 EXECUTIVE SUMMARY 9
2 CCGVIS VISUALIZATION TOOL 10
2.1 STATE OF THE ART IN VISUALIZATION 10
2.2 OVERVIEW OF CCGVIS 10
2.3 VISUALIZATIONS IN CCGVIS 10
2.3.1 2D Slice 10
2.3.2 3D Orthoslice 13
2.3.3 Volume Rendering 17
2.3.4 2D Parallel Comparison 19
2.3.5 3D Parallel Comparison 20
2.3.6 3D Superimposed Comparison 21
2.3.7 Graphical visualization 22
2.4 REGISTRATION IN CCGVIS 23
2.5 CCGVIS ARCHITECTURE 24
2.5.1 Software description 24
2.5.2 CCGVis Program Structure 25
2.6 CCGVIS EVALUATION 27
2.7 CONCLUSIONS AND OUTLOOK 45
3 NEPHROBLASTOMA IMAGE SEGMENTATION 46
3.1 STATE OF THE ART IN TUMOUR IMAGE SEGMENTATION 46
3.2 TUMOUR EXTRACTION 48
3.3 EVALUATION OF THE SEGMENTATION METHOD 51
3.4 CONCLUSIONS AND OUTLOOK 55
4 TIMELINE VISUALIZATION 56
5 REFERENCES 60

Figures

Figure 2-1 2D slice visualization of nephroblastoma patient, showing labelled tumour (red) as transparent coloured overlay. Transverse projection. 11

Figure 2-2 2D slice visualization of nephrobalstoma patient: sagittal projection 12

Figure 2-3 2D slice visualization of nephrobalstoma patient: coronal projection 12

Figure 2-4 3D orthoslice visualization, showing nephroblastoma image in 3 orthogonal planes and labelled tumour as transparent coloured isosurface: pre-treatment 13

Figure 2-5 3D orthoslice visualization, showing nephroblastoma image in 3 orthogonal planes and labelled tumour as transparent coloured isosurface: post-treatment 14

Figure 2-6 3D orthoslice visualization, showing nephroblastoma image and tumour as single plane in arbitrary orientation. The slice direction is controlled by sliders which rotate the plane about the image x and y axes 15

Figure 2-7 3D orthoslice visualization, showing lung image in single plane and labelled tumours as transparent coloured isosurfaces 15

Figure 2-8 orthoslice visualization, showing glioblastoma image in single plane and labelled tumour as transparent coloured isosurface. The segmentation contains multiple labelled components. 16

Figure 2-9 Cumulative effect of transparent layers on ray colour. The colour of white light reflected from two transparent triangles depends on the depth order of the triangles. 16

Figure 2-10 Volume rendering visualization showing torso as semi-transparent block with mesh tumour embedded. 17

Figure 2-11 Volume rendering visualization showing torso as semi-transparent block. The range thresholds have been set to show the kidneys and the tumour (purple)..... 18

Figure 2-12 2D parallel comparison of real and simulated nephroblastoma tumours, showing (left) real post-treatment tumour and (right) simulated tumour. 19

Figure 2-13 3D parallel comparison of real and simulated nephroblastoma tumours, showing (left) real post-treatment tumour and (right) simulated tumour. 20

Figure 2-14 3D superimposed comparison visualization of nephroblastoma, showing baseline simulated tumour at day 0 (yellow) with simulated tumour at day 29 (green)..... 21

Figure 2-15 3D superimposed comparison visualization of nephroblastoma, showing real post-treatment tumour (red) with simulated tumour at day 29 (green). 22

Figure 2-16 Plot of simulated tumour volume vs time; the red crosses are real tumour volumes. 22

Figure 2-17 Images of nephroblastoma patient before registration. Left: post-treatment (unregistered); right: pre-treatment. 24

Figure 2-18 Images of nephroblastoma patient after registration. Left: post-treatment (registred); right: pre-treatment. 24

Figure 2-19 CCGVis program structure..... 25

Figure 3-1 Illustration of different processes of the method. Top left: 3D MRI image. Top right: 2D slice for expert user selection of tumour seeds. Bottom left right: segmentation results of 2D slice. Bottom right: segmentation result 3D MRI..... 49

Figure 3-2 Graph construction. The red and blue dots represent the pixels in the image grid. The red and blue planes represent the labels of foreground and background to which the pixels are to be assigned. The thickness of the red and blue lines represents the strength of the link between the pixels and the labelled seed points. 50

Figure 3-3 User section of tumour seeds. (a) The user select an ROI (tumour seeds) in red circle in one of the image slices. (b) The segmentation results of the methods in all the slices. (c) Images manually-labelled by experts. 51

Figure 3-4 Box plots of Dice coefficient, RMSE, TNR and TPR of results evolution on the 48 MRI scans. 53

Figure 3-5 Segmentation results. Row (a): left 2D MRI image, right: 3D scan. Row (b): left segmentation result in 2D (in green), right: segmentation result in 3D (in green). Row (c): left experts hand labelled in 2D (in red), right: experts hand labelled in 3D (in red). Row (c): left overlap of the segmentation result and the experts hand labelled in 2D, right: overlap of the segmentation result and the experts hand labelled in 3D. 54

Figure 3-6 Segmentation results before and after radio-chemotherapy. Column (a): 2D MRI images, the segmentation results in green and in red experts hand labelled before therapy. Column (b): corresponding 3D images, the segmentation results green and in red experts hand labelled before therapy. Column (c): 2D MRI images, the segmentation results in green and in red experts hand labelled after therapy. Column (c): corresponding 3D images, the segmentation result green and in red experts hand labelled after therapy. 55

Figure 4-1 Timeline visualization of medical database 56

Figure 4-2 Effect of zoom on timeline, showing more detail in a narrower time range..... 57

Figure 4-3 Effect of drag left-right, interactively moving along the timeline..... 57

Figure 4-4 Clustering of close-by items to avoid clutter. 58

Figure 4-5 Colour coding of items. 58

Figure 4-6 Content description, including thumbnail images. 59

Figure 4-7 Content description showing download link. 59

Tables

Table 3-1 Performance evaluation of our segmentation algorithm on 48 multi-sequence MRI scans. Using sensitivity (TPR), specificity (TNR), false positive rate (FPR), false negative rate (FNR) and the accuracy (ACC) with their respective standard deviations and 95% confidence interval..... 52

Table 3-2 Performance evaluation of our segmentation algorithm on 48 multi-sequence MRI scans. Using dice coefficient, root-mean-square (RMSE), and jaccard index with their respective standard deviations and 95% confidence interval. 52

1 Executive Summary

The CHIC project aims to create new technology in the modelling of cancer. As part of this process, the models and hypermodels which have been developed in CHIC must be compared with ground truth to answer the question: did a particular model correctly predict the evolution of a tumour during treatment? This requires a tool which can visualize the simulated tumour along its timeline, and compare this with the corresponding real pre- and post-treatment tumour, to assess the validity of the simulation.

Section 2 of this document describes a visualization tool called CCGVis which was developed to fill this need. CCGVis is a desktop tool for visualizing and comparing tumours and simulations. CCGVis can import, register and visualize medical data, segmentation data and simulations. Images can be imported singly, in image/segmentation pairs, or as time series. Visualizations include slice and orthoslice views in 2D and 3D, isosurfaces in 3D, volume rendering, comparisons between real and simulated tumours, and plots of tumour growth. Section 2.3 describes the CCGVis visualizations in detail, Section 2.4 describes the image registration in CCGVis, Section 2.5 describes the software architecture, and Section 2.6 describes an evaluation of CCGVis.

In order to assess a tumour in a medical image, it is necessary to segment the image – that is, to label the voxels in the image which belong to the tumour. Manual segmentation is a skilled task and very labour-intensive, so automatic and semi-automatic methods are much-needed. Segmentation is particularly difficult in the case of nephroblastoma because the tumours can be heterogeneous, can have low contrast with the surrounding tissue, and be highly variable in appearance from patient to patient. Section 3 presents a semi-automatic segmentation algorithm for nephroblastoma tumours.

The clinical database in CHIC is complex, featuring medical images, segmentations and simulations. In Section 4 we present work on a multiscale timeline visualization for medical data, in which the items are presented on a timeline, classified by colour and clustered to reduce clutter.

2 CCGVis Visualization Tool

2.1 State of the art in visualization

The current state-of-the-art in terms of visualization library software is VTK (www.vtk.org). This library provides importers for most image and graphics formats, and a comprehensive variety of visualization components, including some information visualization in the latest versions. It is easy for developers to add extension classes for their own needs to the VTK framework. Most visualization platforms are based on VTK.

A significant shortcoming of VTK is that its Dicom importer has very limited functionality. The closely-related library ITK (www.itk.org), which specializes in medical image segmentation, is often used with VTK when both segmentation and visualization are required; ITK has full Dicom functionality, and integrates with VTK, so for this reason alone is a useful component of a visualization system. ITK also includes a framework and variety of algorithms for image registration.

VTK has no serious rival for constructing visualizations with images and 3D graphics, but is a relative newcomer to the field of information visualization. Therefore other libraries such as Qwt may provide higher quality visualizations of graphs and charts.

Although there is good visualization software available in terms of library components, the availability of freely-available and extensible API's, such as MAF (http://www.openmaf.org) and DrEye (http://biomodeling.ics.forth.gr/?page_id=8), is very limited. Maf is an extremely adaptable and programmable platform which has supported a wide variety of VPH projects, but has not been in active development for a number of years. DrEye is a flexible platform which is already central to the CHIC project – it is extensible mainly by the addition of external programs which can be integrated as "plugins". Currently, no API platform exists which supports the visualization and comparison of both medical and simulation data.

2.2 Overview of CCGVis

CCGVis is a desktop tool for visualizing and comparing tumours and simulations. CCGVis can import, register and visualize medical data, segmentation data and simulations. It can import various formats, including dicom, mha, nifti and CHIC simulations. Images can be imported singly, in image/segmentation pairs, or as time series. Metadata containing information about the segmentation labelling and the image projection can be added in the form of json files. Visualizations include slice and orthoslice views in 2D and 3D, isosurfaces in 3D, volume rendering, comparisons between real and simulated tumours, and plots of tumour growth. Images and video can be saved to file with captions for later reporting. CCGVis can be executed as a standalone desktop application, or it can be launched from another application with command-line arguments. Input and output data is exchanged via the local file system, in directories specified by the command line arguments.

The API consists of a display window, a widget panel for interactive control, and menus for loading data and launching visualization tasks.

2.3 Visualizations in CCGVis

2.3.1 2D Slice

The CCGVis slice view is shown in Figure 2-1. The medical image is presented as a 2D slice, and the segmentation labelling is shown as a transparent coloured overlay. The tumour volume in ml is calculated from the segmentation image and displayed in the control panel.

The input for this visualization is an image/segmentation "pair", that is, a medical image and its corresponding segmentation image containing a labelling of the voxels. Segmentation images are typically binary, but can also contain multiple labels to represent different tissues and tumour

components. In CCGVis, the labels present are automatically calculated from the segmentation image, or they can be listed and named in a json metadata file. The metadata file can also contain the projection information, mapping the images axes to the patient axes. In the absence of metadata, the image-patient mapping can be adjusted by the user from the control panel.

The overlay is generated by a combination of two VTK filters: vtkImageMapToColors, which converts the segmentation image into an image with colours and transparency as set by the control panel; and vtkImageBlend, which mixes the overlay and medical images according to their relative transparencies.

Figure 2-2 and Figure 2-3 show the same image in the sagittal and coronal projections.

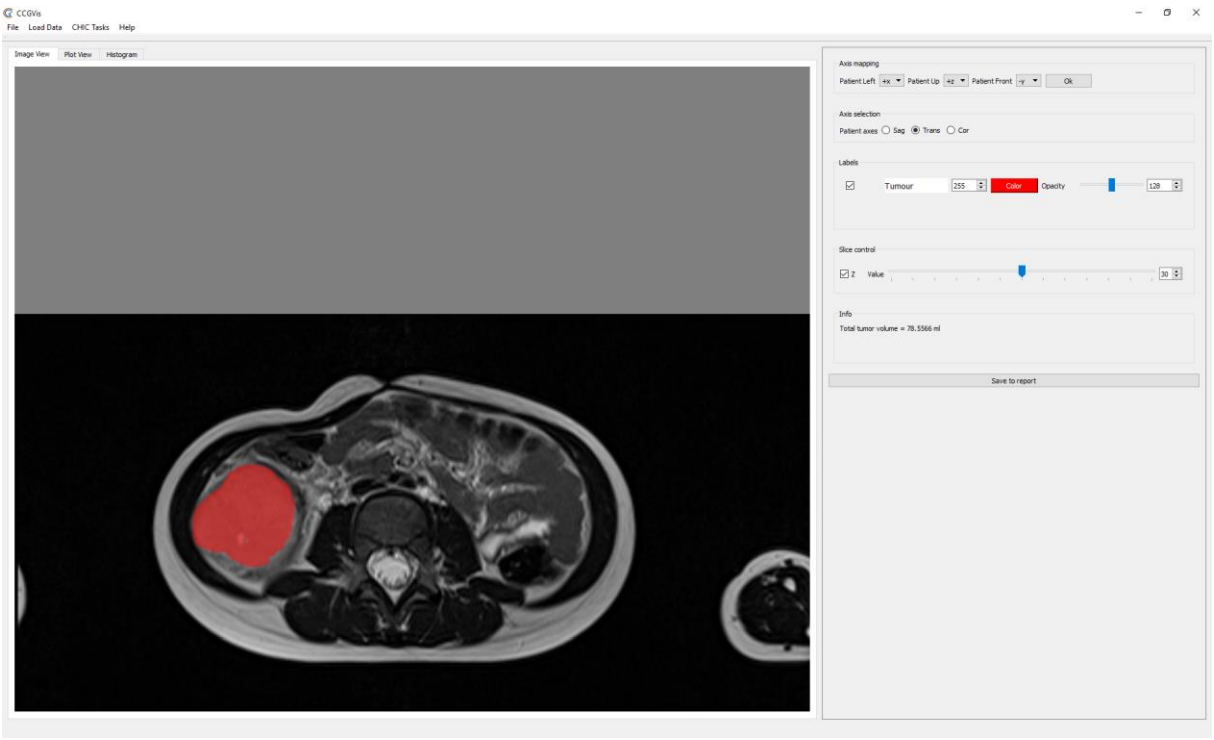

Figure 2-1 2D slice visualization of nephroblastoma patient, showing labelled tumour (red) as transparent coloured overlay. Transverse projection.

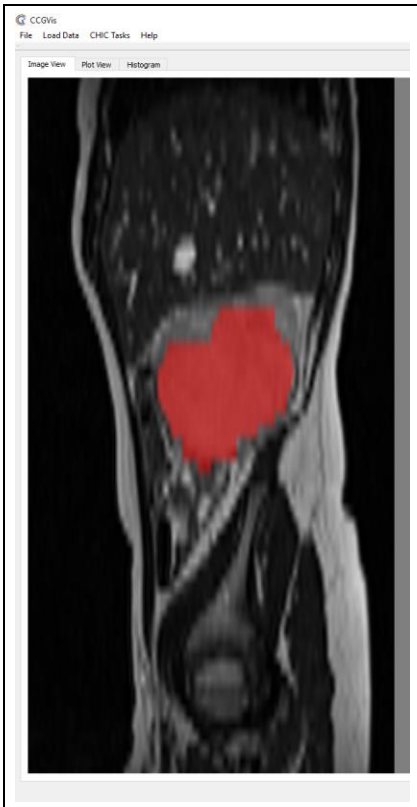

Figure 2-2 2D slice visualization of nephroblastoma patient: sagittal projection

Figure 2-3 2D slice visualization of nephroblastoma patient: coronal projection

2.3.2 3D Orthoslice

The 3D orthoslice visualization presents the medical image as a slice or a set of orthogonal slices in 3D space. The tumour is visualized in 3D space as an isosurface: that is, a mesh representation of the contour boundary in the segmentation image. The isosurface is generated by the marching cubes algorithm (Lorensen & Cline, 1987). The advantage of the orthoslice view is that it presents the 3D interior of the patient very well, but is at the same time open and uncluttered. Figure 2-4 shows an orthoslice view of the nephroblastoma shown previously in Figure 2-1.

CCGVis can load image series datasets. Figure 2-4 and Figure 2-5 show the pre-treatment and post-treatment images of the nephroblastoma. The qualitative shrinkage in the tumour is evident in the images, and can be read quantitatively in ml from the control panel on the right.

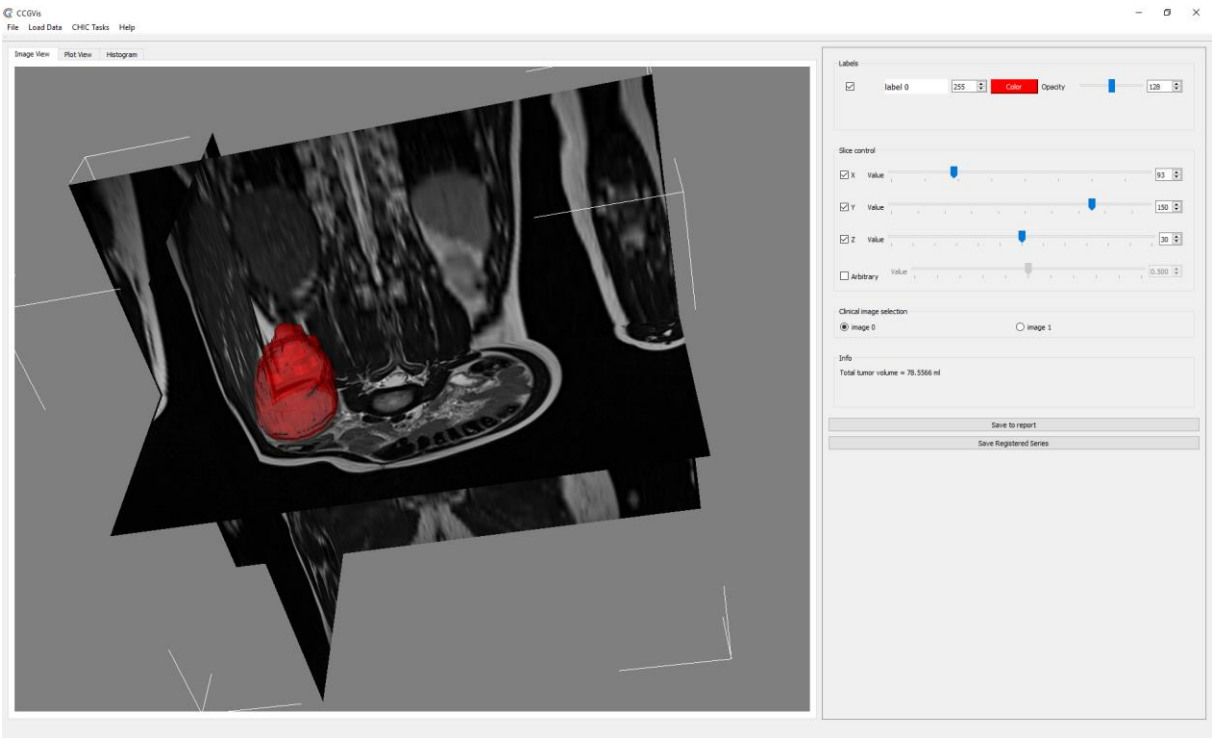

Figure 2-4 3D orthoslice visualization, showing nephroblastoma image in 3 orthogonal planes and labelled tumour as transparent coloured isosurface: pre-treatment

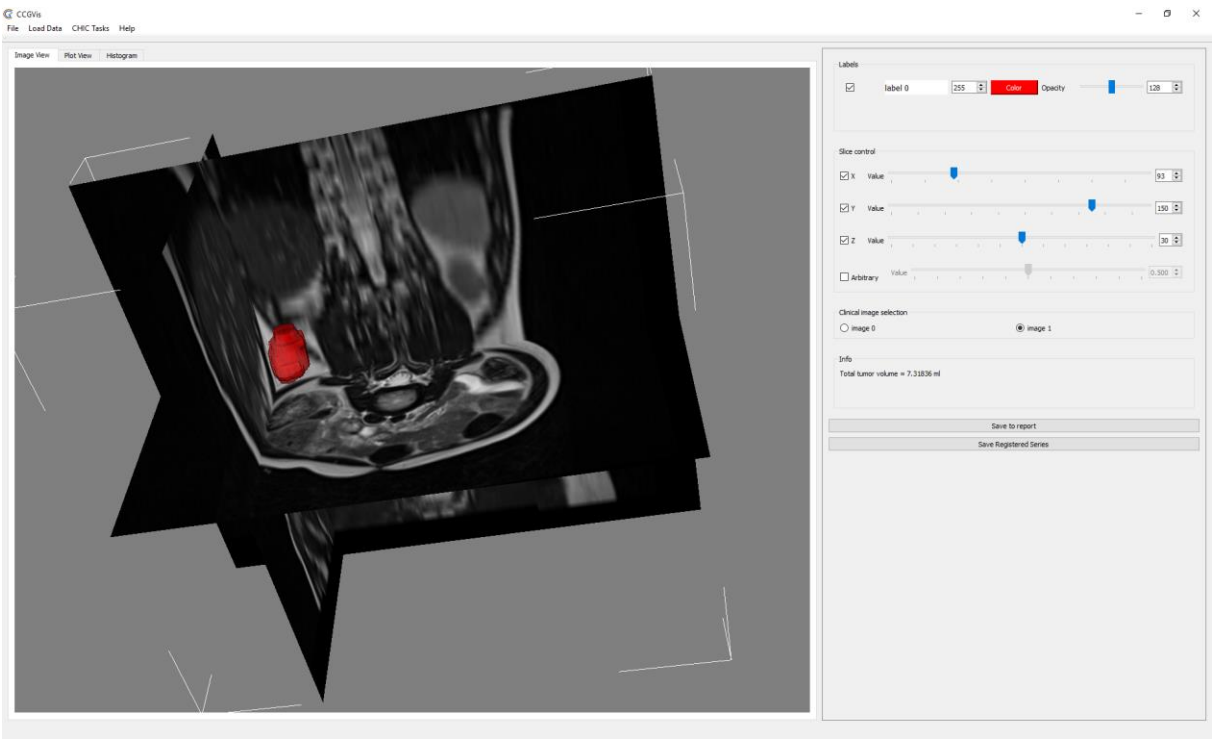

Figure 2-5 3D orthoslice visualization, showing nephroblastoma image in 3 orthogonal planes and labelled tumour as transparent coloured isosurface: post-treatment

The orthoslice view also allows the user to display a slice in an arbitrary orientation, as shown in Figure 2-6. The orientation can be rotated about the image x and y axes using sliders in the control panel. The position of the slice is defined by a parameter $\lambda = [0,1]$ where 0 and 1 correspond to the extrema of the image box as projected onto the normal direction of the slice.

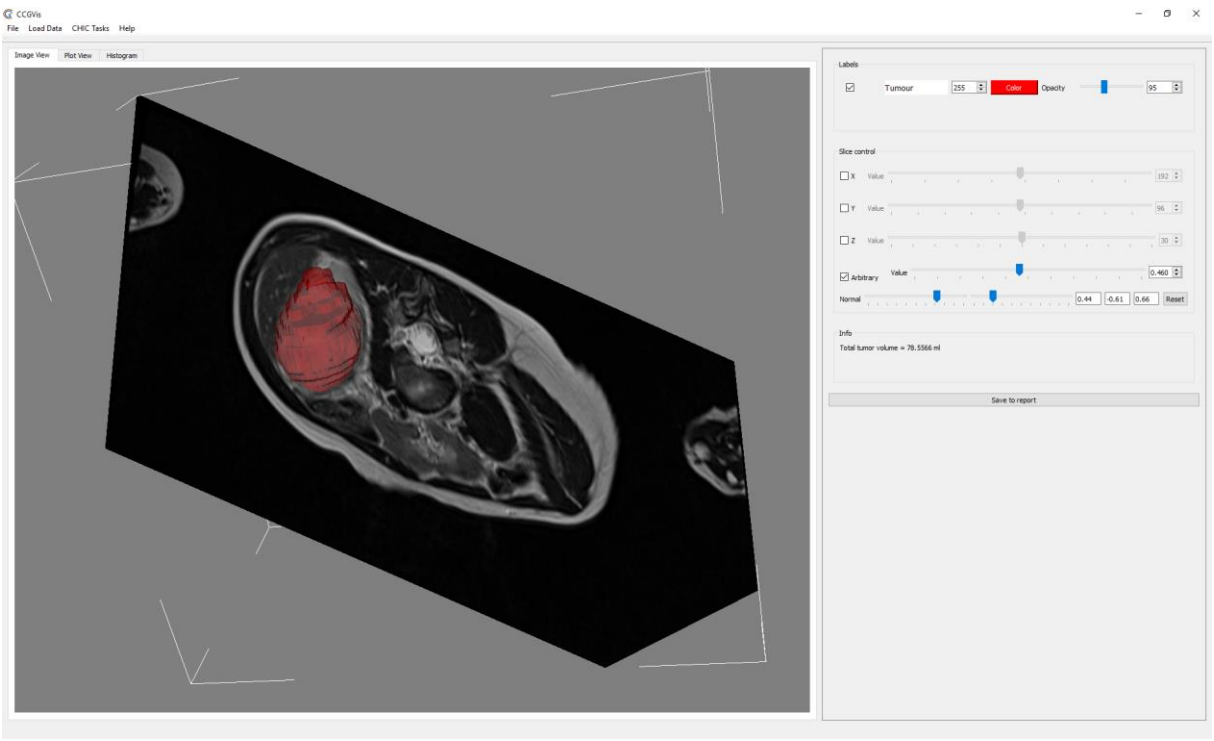

Figure 2-6 3D orthoslice visualization, showing nephroblastoma image and tumour as single plane in arbitrary orientation. The slice direction is controlled by sliders which rotate the plane about the image x and y axes.

Figure 2-7 shows the 3D orthoslice view (one slice only) applied to lung cancer. Two tumours are visible.

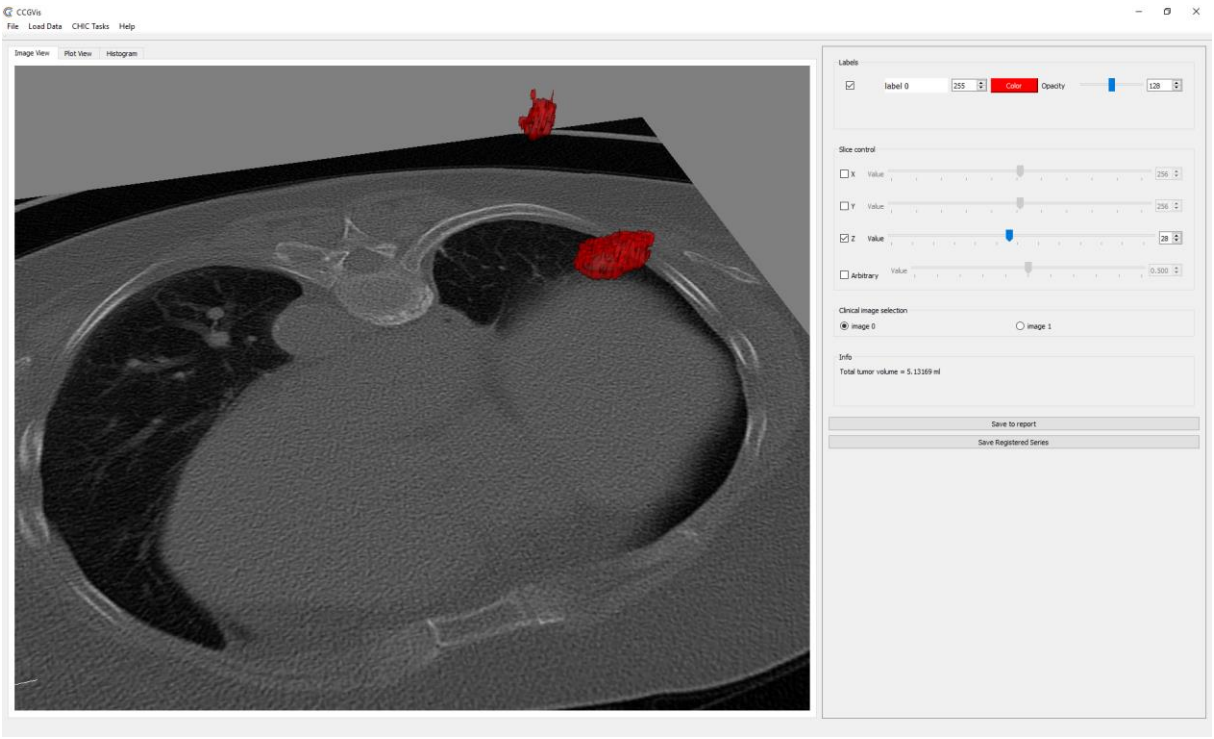

Figure 2-7 3D orthoslice visualization, showing lung image in single plane and labelled tumours as transparent coloured isosurfaces

Figure 2-8 shows a brain tumour as a 3D slice. In this case, the segmentation contains multiple labels corresponding to different components of the tumour: the large green volume corresponds to

oedema, the red to necrosis, and the yellow and blue to enhancing and non-enhancing tumour tissue.

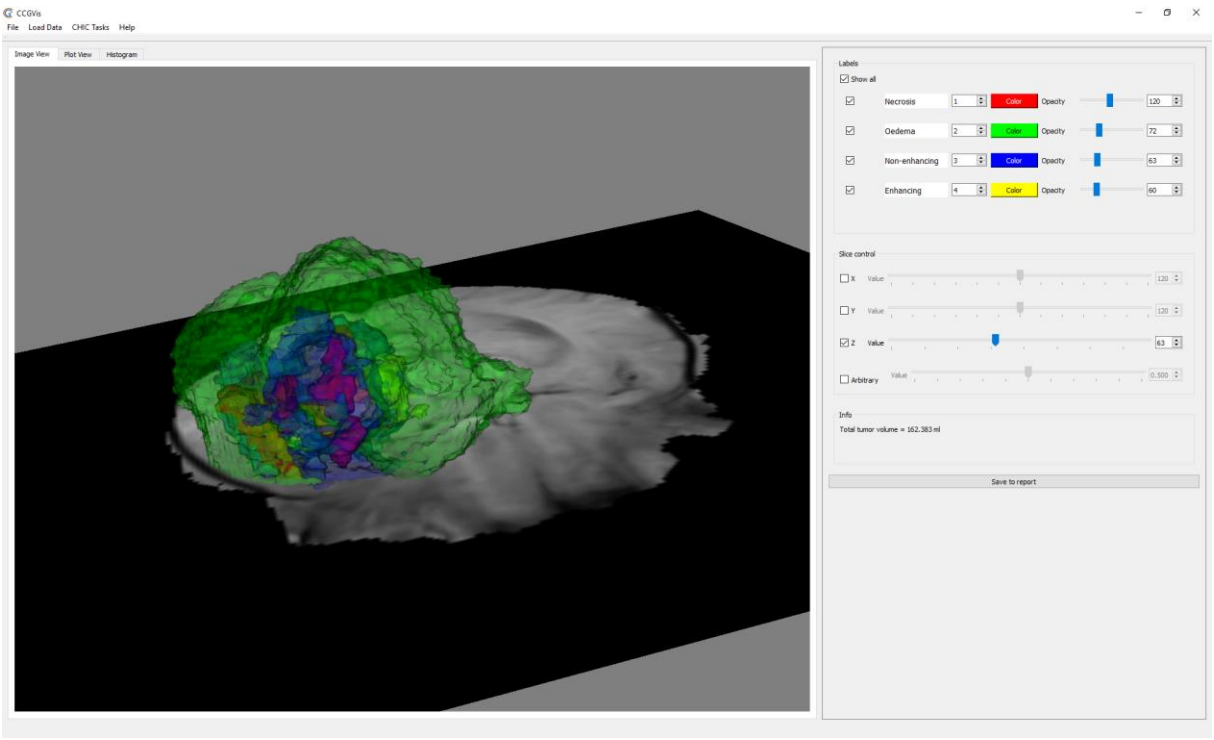

Figure 2-8 orthoslice visualization, showing glioblastoma image in single plane and labelled tumour as transparent coloured isosurface. The segmentation contains multiple labelled components.

With multiple surfaces occluding and nesting each other, it is important that the transparency works well. Transparency in computer graphics is computationally expensive to calculate because the rendered colour of transparent layers depends on the depth order of the layers. This is illustrated in Figure 2-9. White light is incident on two triangles T_1 and T_2, with respective colours C_1 and C_2, and opacities A_1 and A_2. To calculate the cumulative colour at the eye, it is necessary to know the depth order of the triangles.

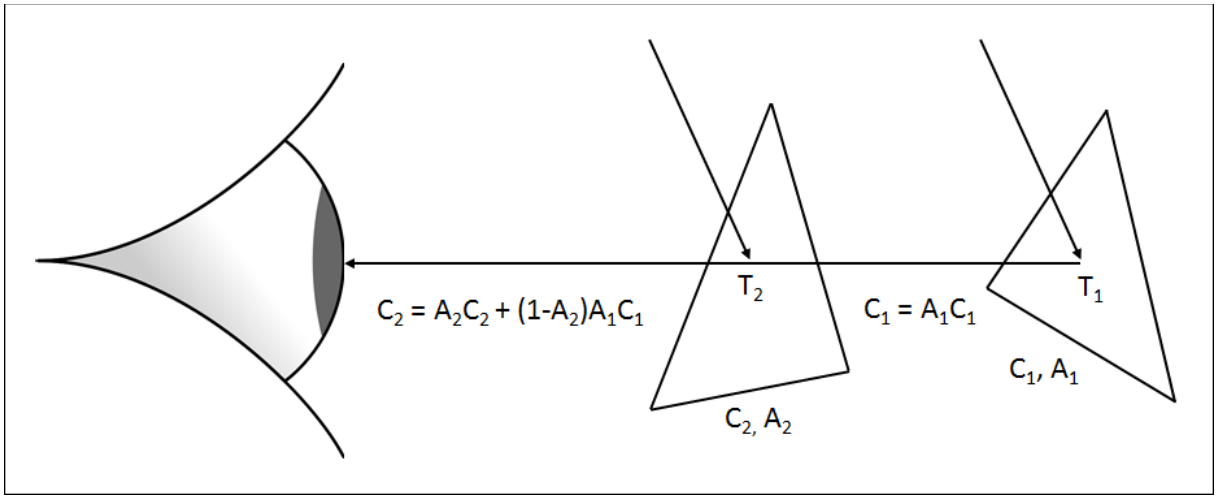

Figure 2-9 Cumulative effect of transparent layers on ray colour. The colour of white light reflected from two transparent triangles depends on the depth order of the triangles.

The simplest method of resolving this problem is simply to sort the triangles into depth order before rendering. VTK provides a filter to perform this task. However, sorting large numbers of triangles is computationally expensive. Also, in order to sort triangles which belong to different meshes in the

scene, the meshes must be merged into one, adding to the computation time and losing the ability to process the meshes independently.

A better method supported by VTK is depth peeling (Everitt, 2001). This works on the whole scene and does not require the meshes to be merged and sorted. The standard graphics pipeline features a depth buffer, which for each pixel contains the depth of the nearest surface to the camera. Where there is no transparency, this efficiently removes occluded surfaces from further processing. However, when transparency is present, all the surfaces must be composited: the nearest, second-nearest, third nearest and so on. Depth peeling works by rendering the nearest surfaces as normal, but then uses the depth buffer to remove the nearest surface, leaving the second nearest. The second nearest surface is then rendered and blended with the first. The second nearest is now removed, and the third nearest rendered and blended, and so on until no more depth layers remain. The iterative algorithm can be computationally expensive, but this has not been a problem in CCGVis.

A problem with depth peeling in the VTK implementation arises when there are coincident surfaces in the scene. When two mesh fragments are at the same depth, one is used and the other discarded, rather than the two being blended. This is a major problem for CCGVis, since it is often the case that near-identical surfaces are being compared. The solution in CCGVis is to dither the positions of the mesh points by a tiny random amount, not visible to the eye but enough to separate the meshes and allow the algorithm to work properly.

2.3.3 Volume Rendering

The volume rendering visualization in CCGVis shows the whole image as a 3D semi-transparent block. The location of the tumour is shown by the same isosurface mesh as seen in the 3D orthoslice view in Section 2.3.2. The rendering is generated by the VTK filter vtkGPUVolumeRayCastMapper, and the transfer function – the mapping between image intensity and rendered colour – is a linear ramp of hue, with the darkest image intensity mapped to violet and the brightest to red. All voxels have the same global opacity. A volume rendering of the nephroblastoma patient is shown in Figure 2-10.

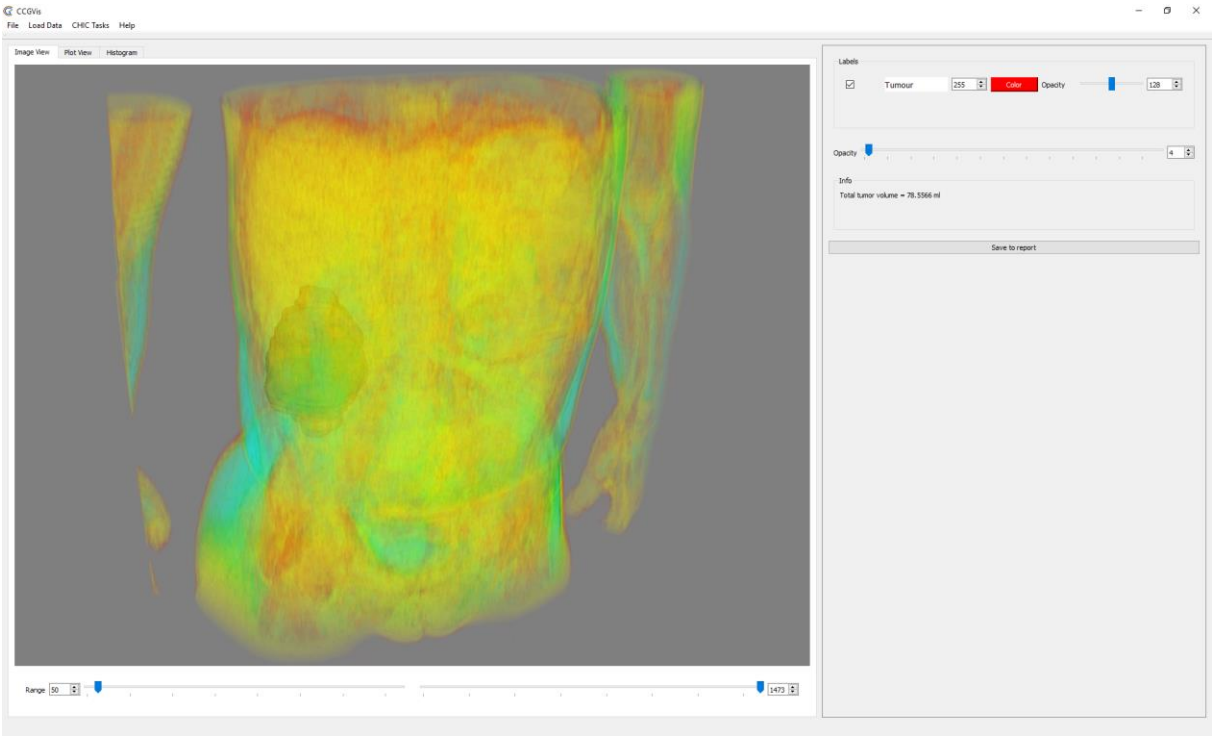

Figure 2-10 Volume rendering visualization showing torso as semi-transparent block with mesh tumour embedded.

CCGVis provides two controls for manually adjusting the transfer function: an opacity slider for setting the global opacity, and a pair of range sliders for setting the minimum and maximum values for the range of grey levels to view – effectively a windowed threshold on the image. The hue range from violet to red is compressed into the range selected. By setting the sliders, it is possible to focus on particular tissues. Figure 2-11 shows the volume rendering with the range thresholds set to show the kidneys and the tumour.

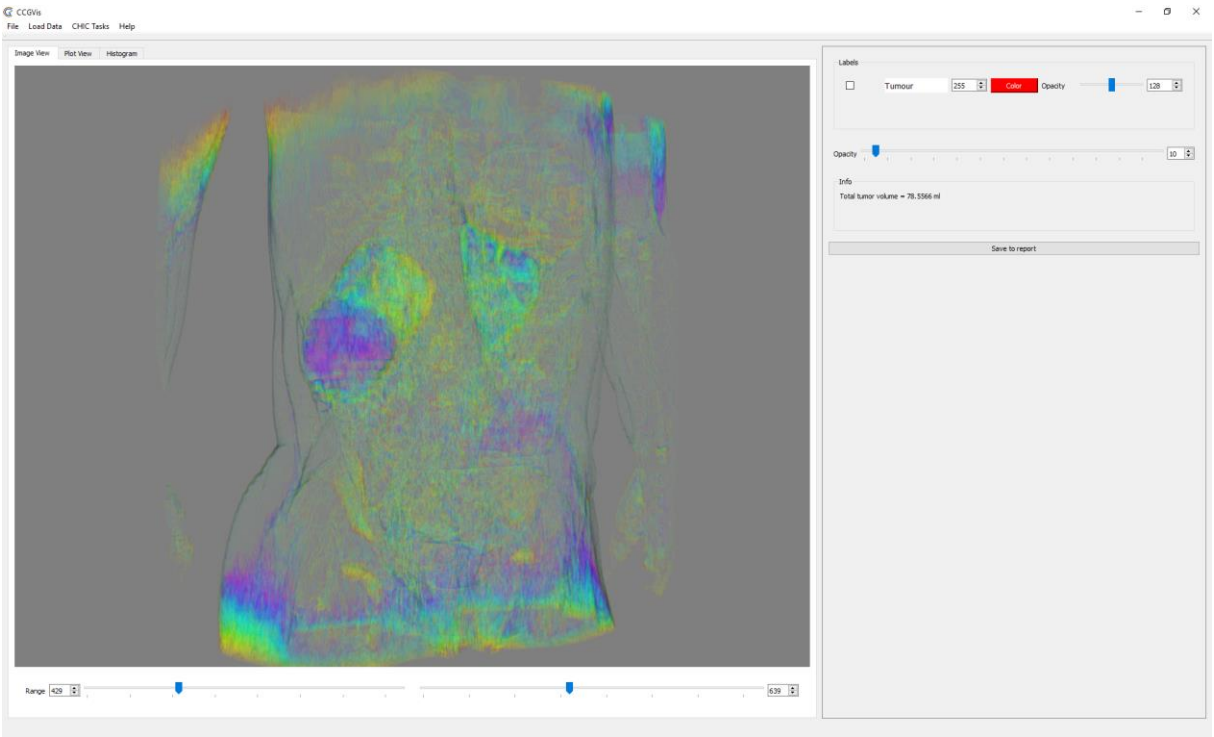

Figure 2-11 Volume rendering visualization showing torso as semi-transparent block. The range thresholds have been set to show the kidneys and the tumour (purple).

2.3.4 2D Parallel Comparison

CCGVis provides several visualizations for the purpose of directly comparing real tumours and their simulations. A video showing these visualizations can be found at https://youtu.be/pR0USCxPwbM. The first such view is the 2D parallel comparison, as shown in Figure 2-12. The visualization shows two 2D slice views (see in Section 2.3.1) side by side. The left image shows the time series of medical images with the real tumour, while the right image shows the simulated tumour. The left time-series image is selected, as in Section 2.3.1, by radio buttons in the control panel. The left image in Figure 2-12 has been set to show the post-treatment tumour. For comparison, the right image shows the simulated tumour; this is always shown embedded in the first time-series image, since this defines the coordinate system. The day number of the simulation is controlled by a time slider in the control panel. Note that the post-treatment image on the left has been registered so that it is in the same coordinate system as the pre-treatment image and simulated tumour on the right. Registration will be described in Section 2.4.

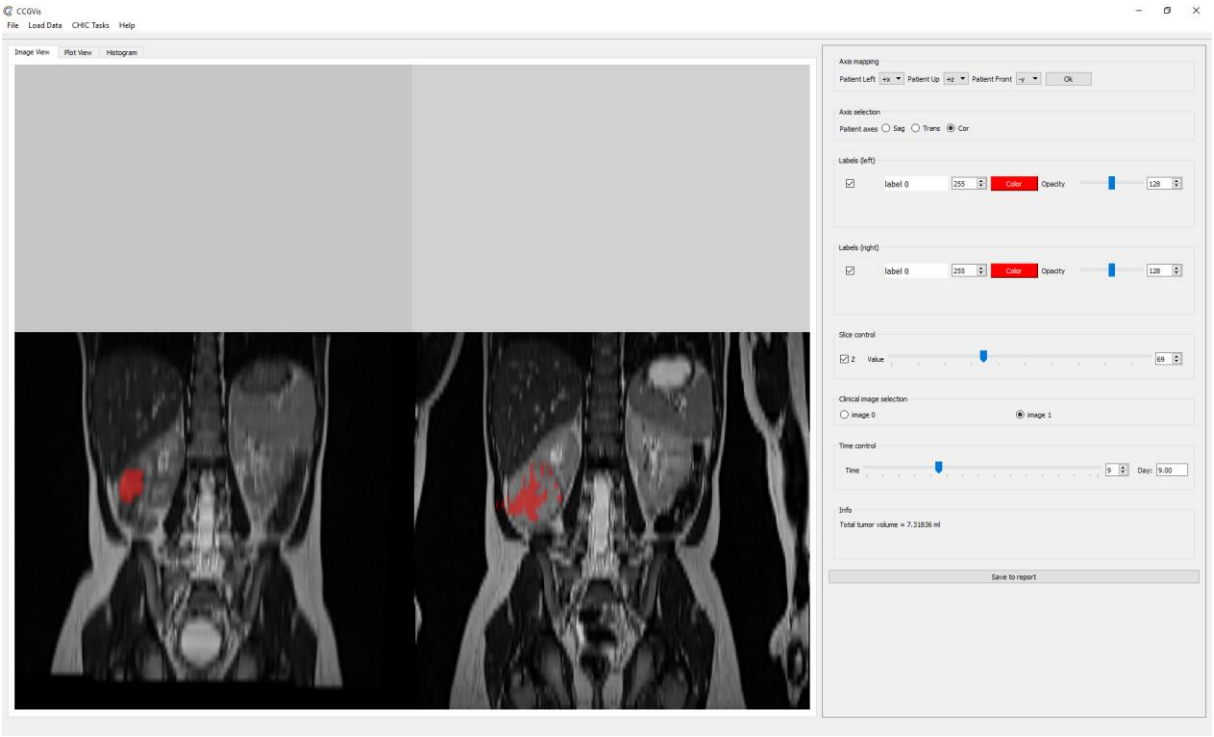

Figure 2-12 2D parallel comparison of real and simulated nephroblastoma tumours, showing (left) real post-treatment tumour and (right) simulated tumour.

2.3.5 3D Parallel Comparison

The 3D parallel comparison is similar to the 2 comparison described in Section 2.3.4, with the real tumour on the left and the simulated tumour on the right, but uses the orthoslice view described in Section 2.3.2. The cameras on the left and right are synchronised so that any rotation or zoom interaction in one is mirrored in the other. The simulation on the right is shown only as an isosurface without the image slice, though the original reason for this – that the control panel would require two sets of slice controls – no longer applies to successfully registered images, and it is likely that future versions of CCGVis will restore the image slice context to the right hand tumour.

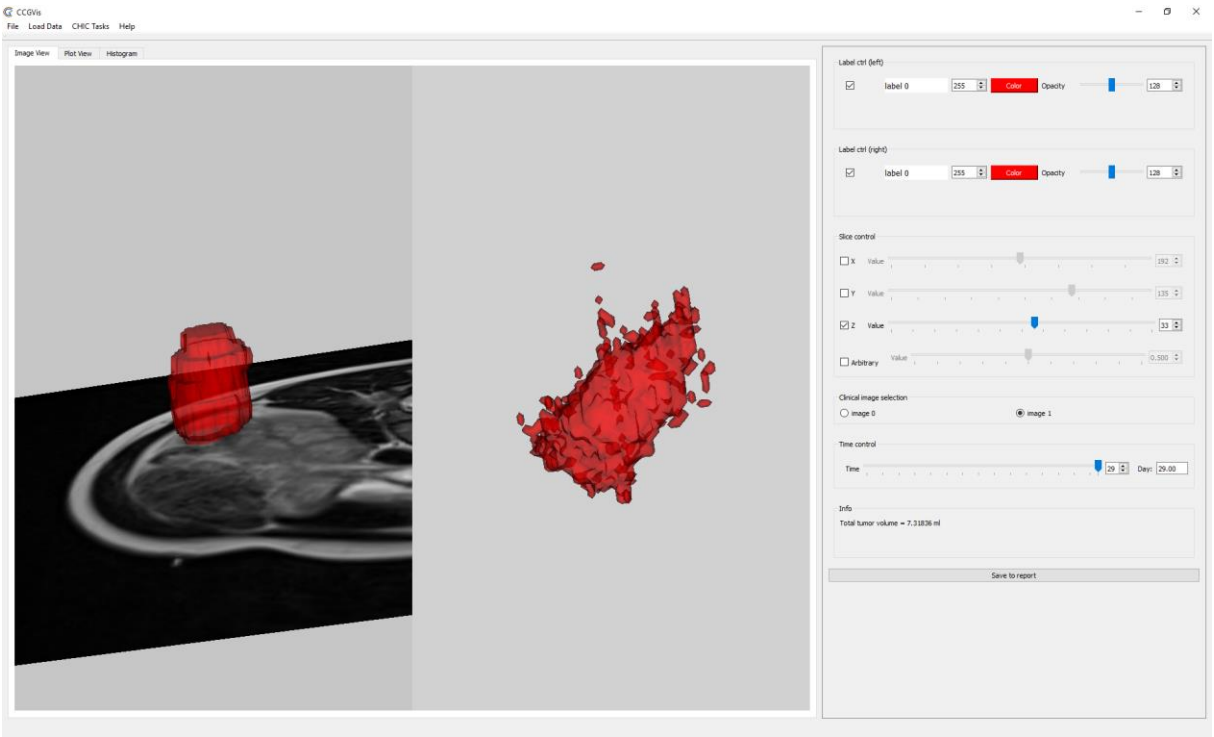

Figure 2-13 3D parallel comparison of real and simulated nephroblastoma tumours, showing (left) real post-treatment tumour and (right) simulated tumour.

2.3.6 3D Superimposed Comparison

The superimposed comparison is a comparison of two or more tumours in the same image space. The visualization is a combination of 3D orthoslice images and isosurface tumours, as in the parallel 3D described in Section 2.3.5, but the tumours to be compared are placed in the same image instead of parallel images. This is a powerful and direct method of comparison. The user is able to select which tumour isosurfaces to enable in the view: the baseline real(0), the baseline simulated(0), the current time-series real(t) and the current time-slider-selected simulated(t). Figure 2-14 shows a comparison between the simulation at day 0 (yellow) and day 29 (green) as transparent isosurfaces. Figure 2-15 shows a comparison between the real post-treatment tumour (red) and the simulation at day 29 (green). Note that the real tumour and the background image has been registered so that it is in the same coordinate system as the simulation. It can be seen that in this case the simulation has not correctly predicted the post-treatment position of the tumour.

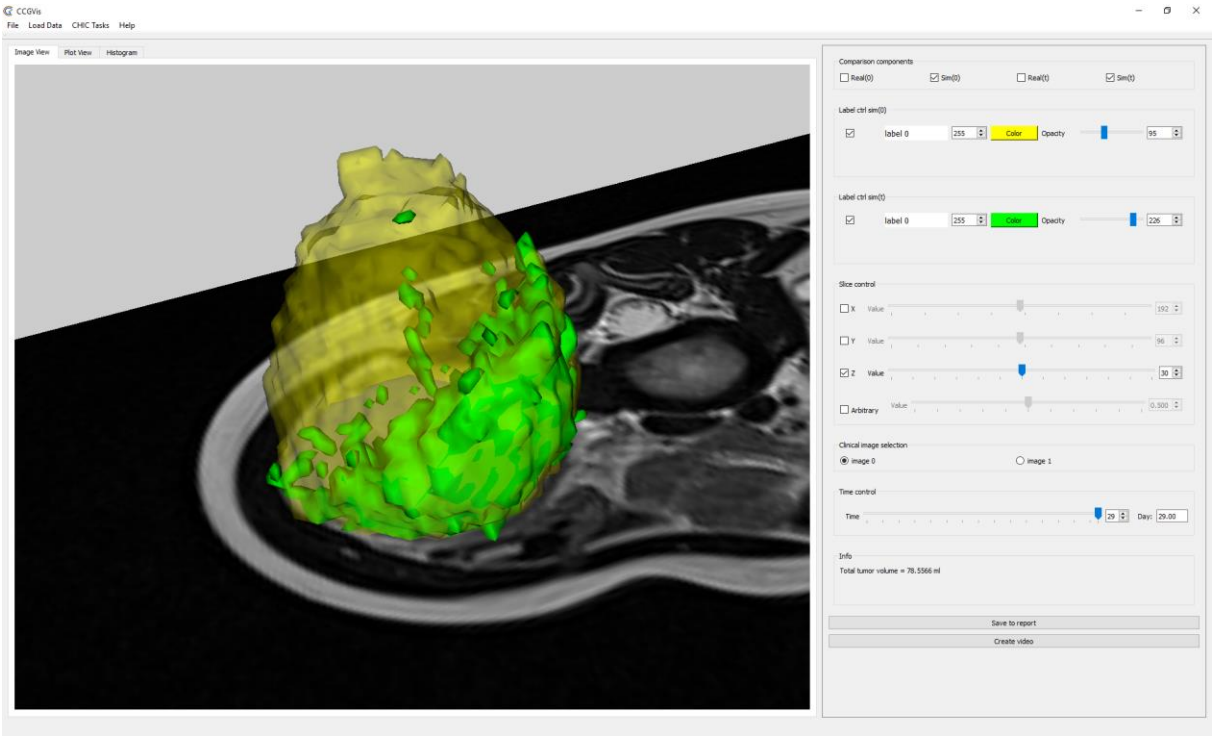

Figure 2-14 3D superimposed comparison visualization of nephroblastoma, showing baseline simulated tumour at day 0 (yellow) with simulated tumour at day 29 (green).

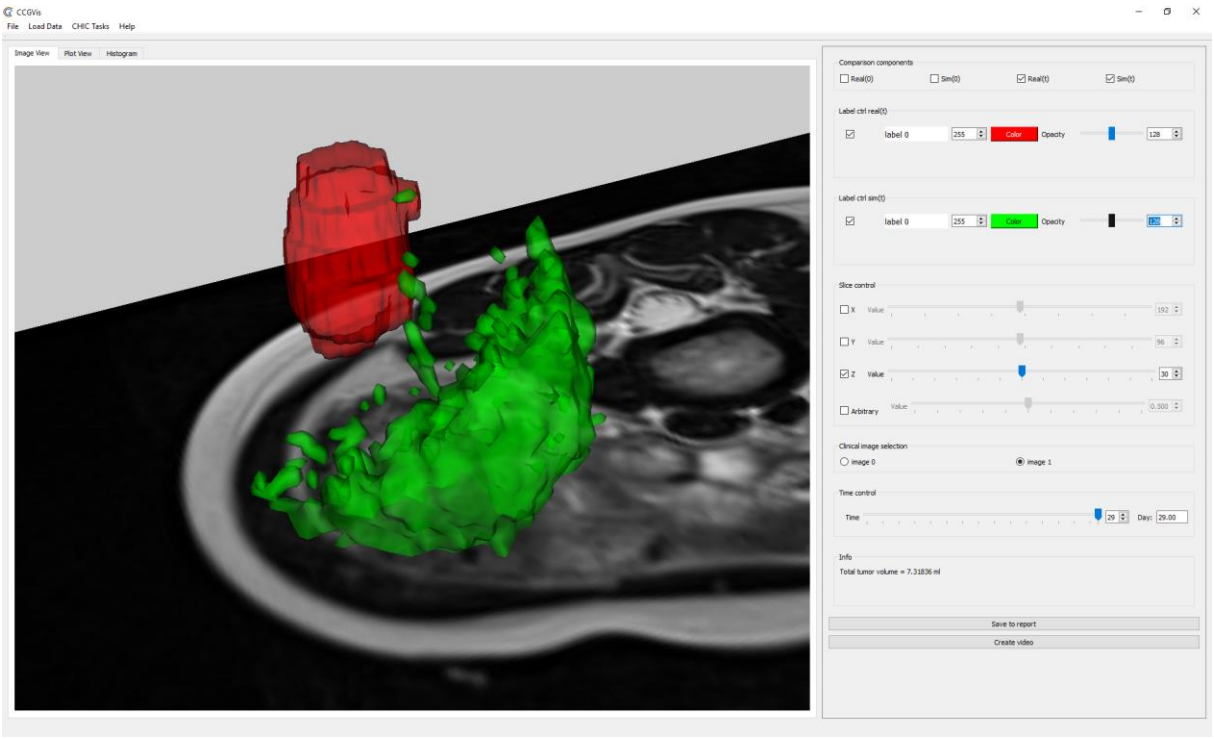

Figure 2-15 3D superimposed comparison visualization of nephroblastoma, showing real post-treatment tumour (red) with simulated tumour at day 29 (green).

2.3.7 Graphical visualization

CCGVis also presents the simulated history of the tumour as a plot of volume against time, as shown in Figure 2-16. This plot shows the shrinkage (and beginnings of regrowth) of a simulated nephroblastoma which has been subject to four chemotherapy treatments. For comparison, the volume of the real tumour (red crosses) is marked on the same plot.

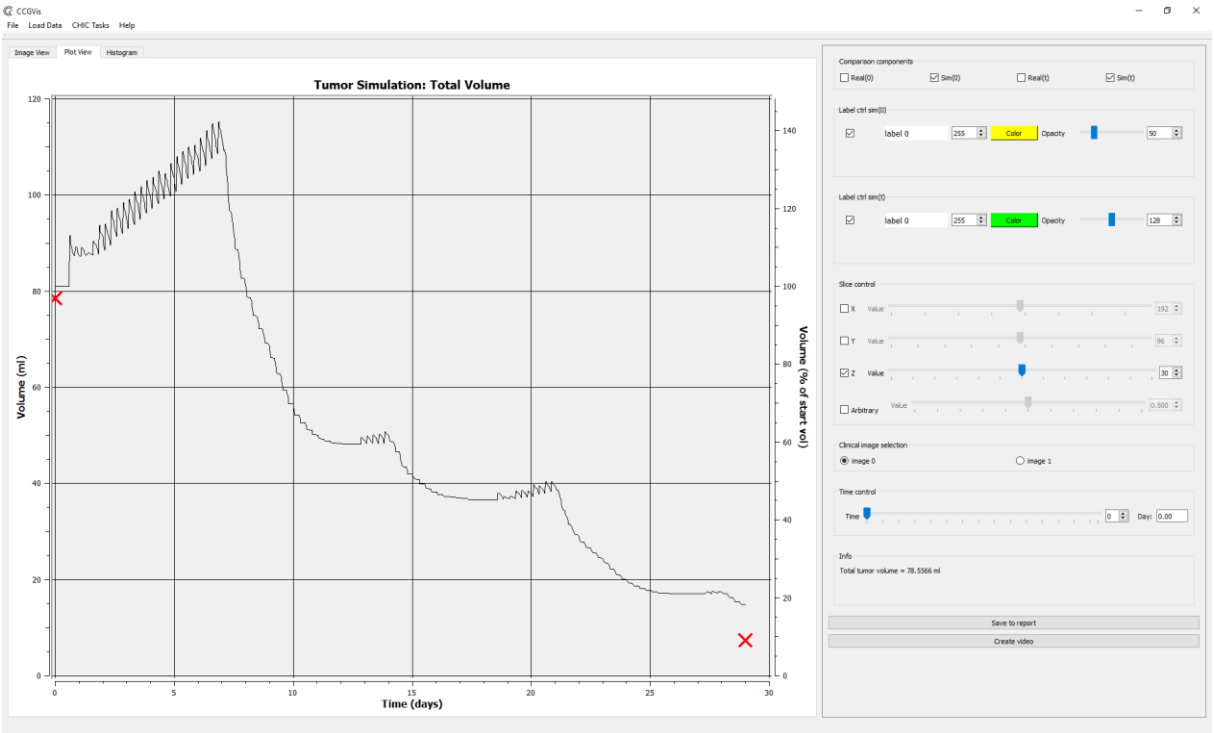

Figure 2-16 Plot of simulated tumour volume vs time; the red crosses are real tumour volumes.

2.4 Registration in CCGVis

When a time-series of medical images is loaded, the images in the set must be registered so that corresponding features have the same coordinates in all the images. This is very important for comparing tumours at different times in the patient's treatment, because registration makes it easier to compare two images by displaying the same anatomy in the same place and on the same slice, and makes it possible to display both pre- and post-treatment tumours in the same image space for direct comparison. The image sequences are registered such that the first image in the series is fixed, and the others are registered against it. The constraint that the first image is always fixed can be sub-optimal if the first image happens to be low-resolution, forcing the rest of the images to be reduced in resolution to match, but it is necessary because the CHIC simulations are based on the coordinate system of the first image.

Registration is performed by ITK. The ITK registration framework divides the registration process into four pluggable and interchangeable components, each of which has wide range of options available:

- The *transform* determines the type of transform which is applied to the target image, such as 2D, 3D translation or 3D rigid. In CCGVis a 3D rigid transform is used, that is, a translation and rotation. There can be significant rotation of the patient from one image to the next, so simple translation is not sufficient. The centre of rotation is the centre of the image.
- The *interpolator* determines how the values of voxels at non-grid positions are calculated. Linear interpolation is applied to the target image. However, when the registration is complete, the transform must also be applied to the corresponding segmentation image, and in this case linear interpolation would generate spurious non-binary grey levels at the edges of the labelled object. Hence a nearest-neighbour interpolation must be applied when the segmentation is transformed.
- The *optimizer* is the optimization algorithm which solves the registration. CCGVis uses the optimizer which is designed for the transform space of the 3D rigid transform.
- The *metric* is the measure of difference between the images under a given transform. There are a large number of possible metrics. CCGVis uses the simplest and least computationally-expensive metric – the mean-squared difference between the grey levels.

Example registration results are shown in Figure 2-17 and Figure 2-18.

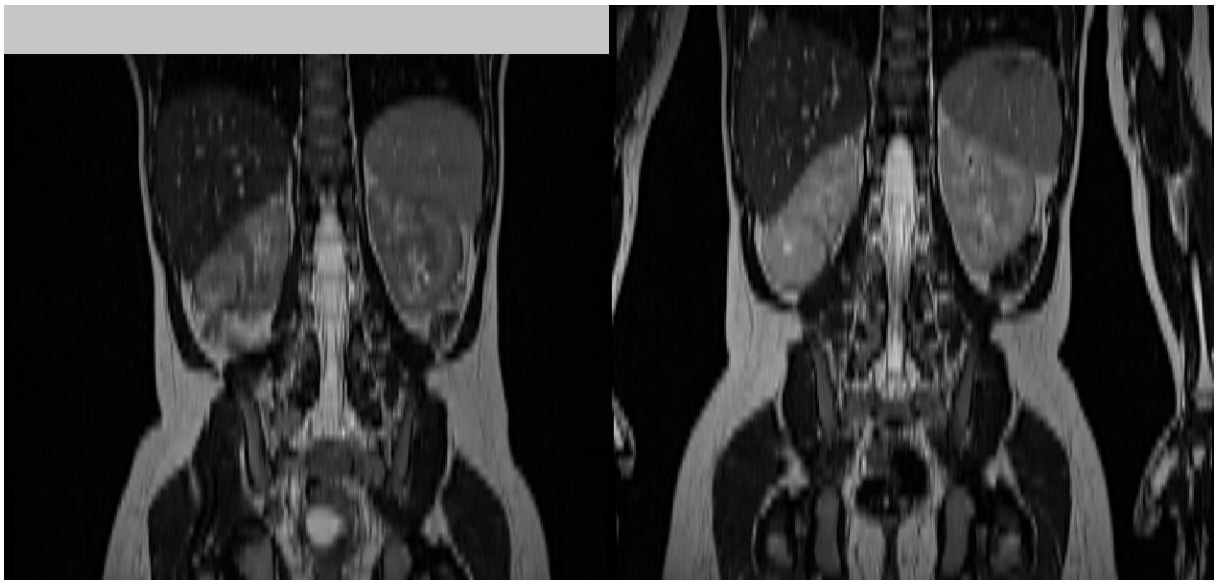

Figure 2-17 Images of nephroblastoma patient before registration. Left: post-treatment (unregistered); right: pre-treatment.

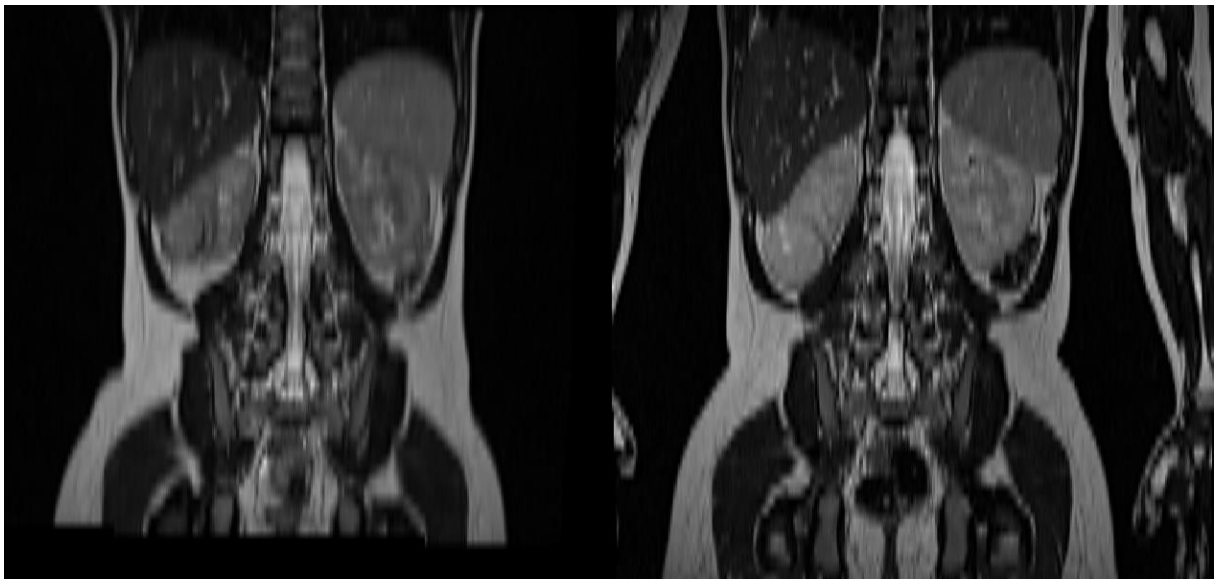

Figure 2-18 Images of nephroblastoma patient after registration. Left: post-treatment (registered); right: pre-treatment.

2.5 CCGVis architecture

2.5.1 Software description

CCGVis is a Windows desktop application which runs on Windows 7-10 or on a Windows emulator such as WineSkin on Mac OS.

CCGVis is written in C++, built using CMake 3.6.2 and compiles as a 32-bit application with Microsoft Visual Studio 2013 or 2015.

CCGVis depends on the following third-party libraries:

- VTK 6.3. The Visualization Toolkit provides much of the graphics software for the visualizations themselves. CCGVis also contains various bespoke VTK filters and bug-fixes.
- Qt 5.5 – 5.6. The Qt library provides basic widgets from which the CCGVis controls are built, and also the framework for event handling.
- ITK 4.7 – 4.9. The Insight Segmentation and Registration Toolkit provides DICOM import functionality and registration software. ITK also provides a framework for image processing.
- Qwt 6.1.2. The Qwt library provides high-quality graph plots and histograms.

2.5.2 CCGVis Program Structure

CCGVis is constructed from modular components as shown in Figure 2-19.

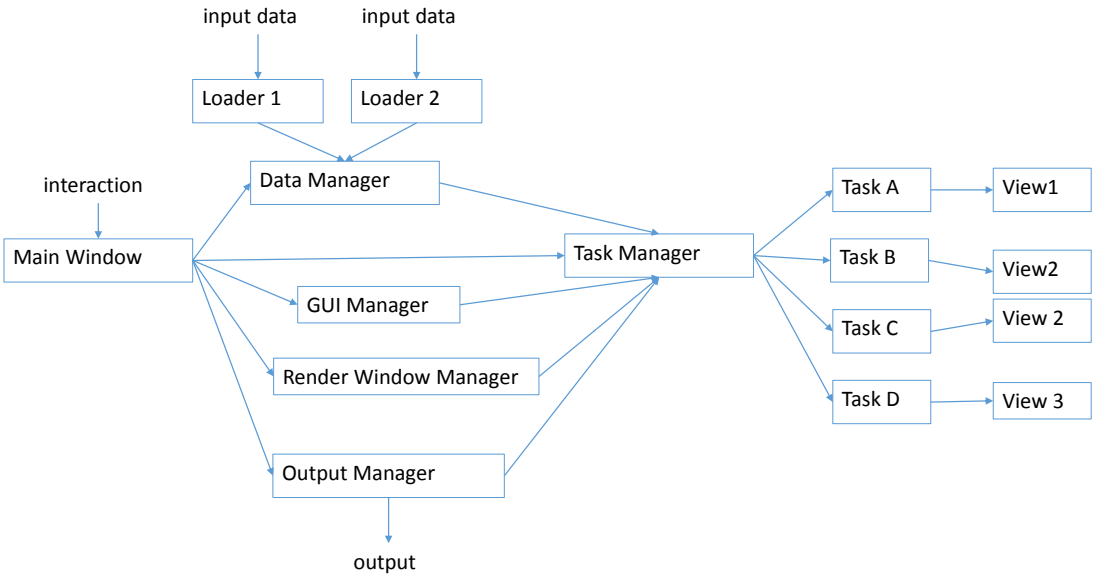

Figure 2-19 CCGVis program structure

- The *main window* is the display and user interface.
- *Loaders* get the input datasets.
- The *data manager* loads, stores and provides datasets on request. Each dataset is a file loader which supplies the vtk readers for the data.
- The *GUI manager* contains the layouts into which tasks can add their widgets.
- The *render window manager* contains the list of render windows in the GUI. It supplies the renderers which correspond to the windows.
- The *output manager* contains utilities for saving output images, plots and video to file.
- The *task manager* executes a task when requested. Currently the tasks are modal: only one task can run at a time.
- A *task* is a visualization (or other executable operation) performed on the data. The task requests its data from the data manager and its renderer from the render window manager.

It connects the data to the visual pipes. It places the GUI components in the main window and connects them to the visual pipes. Typically most of the visual pipes and GUI components will be wrapped in a *view* class.

- A *view* represents a static (i.e. non time-varying) visualization, and contains the visual pipes and the widgets to control it. Views are reusable code which might be used in more than one task.

2.6 CCGVis evaluation

The evaluation exercise consisted of a CCGVis distribution, including example data, and a questionnaire as shown below. A windows batch file with command line arguments was provided which would launch CCGVis with the example data preloaded.

The evaluation was sent to 25 people with varying levels of experience at viewing medical images. Of the 10 respondents, 6 were members of the CHIC project and the remaining 4 were research colleagues from BED. None were directly involved in the development of CCGVis.

The evaluation was based mainly on example data from a nephroblastoma patient, but images of non small cell lung cancer and glioblastoma were also included.

The following is a summary of the responses. For binary questions, the numbers in the boxes show the total number of users who gave the corresponding answer. For questions rated across 5 boxes, bar charts show the distribution of responses.

User details and system requirements

The system requirements are: desktop or laptop running MS Windows or a Windows emulator such as Wineskin on MacOs.

Number of respondents: 10	
Please rate your experience in viewing medical images	none ☐☐☐☐☐expert
Have you used CCGVis before?	Yes 4 No 6
What is your operating system, including any emulator software such as Wineskin?	Windows 7 1 Windows 8 1 Windows 10 6 Virtual Box running Win 10 on MacOs 1 VMWare running Win 8.1 on MacOs 1
Are you using a desktop or a laptop?	Desktop 6 Laptop 4
What is your screen resolution?	The lowest screen resolutions were on laptops at 1366 x 768 and 1280 x 800. No problems arising from lack of screen space were reported.

Launching CCGVis from the command line with pre-loaded data

Run CCGVisRelease.bat.

This should launch CCGVis in full screen with datasets loaded from the command line.

Did CCGVis launch successfully?	Yes 10 No 0

Load Data: View Loaded Datasets

Select "View loaded datasets" from the "Load Data" menu. The filenames appear in the column on the left, and the dataset types in the column on the left.

Are you able to view the list of pre-loaded datasets?	Yes 10 No 0
Are there 6 datasets in the list?	Yes 10 No 0

Tasks: View Image 2D

Select "View image 2D" from the "Tasks" menu. This will display a medical image as a 2D slice.

Are you able to view the medical image in 2D?	Yes 10 No 0
Can you view the image slice-by-slice using the "slice control" slider?	Yes 10 No 0
Can you see the grey tumour within the patient's left kidney? (The kidneys are the bright organs on either side of the spine)	Yes 9 No 1
Is the image displayed in the correct orientation?	Yes 10 No 0
Can you view the image in different projections (sagittal, transverse and coronal) using the axis selection panel?	Yes 10 No 0
Is the image displayed correctly in all three projections? Coronal = patient upright, facing camera Transverse = cross section, spine at bottom Sagittal = side view, patient facing to left	Yes 10 No 0

Tasks: View Image 3D

Select "View image 3D" from the "Tasks" menu. This will display a medical image as a 2D slice floating in 3D space. The mouse is used to interact with the 3D image as follows:

- click and drag = rotate
- right-click and drag = zoom

Are you able to view the medical image slice?	Yes 10 No 0
Can you rotate and zoom the image using the mouse?	Yes 10 No 0
Can you move the slice through the image using the "z" axis slider?	Yes 10 No 0
Can you enable the slices in the "x" and "y" planes so that the image is cut by 3 orthogonal planes (orthoslice view)?	Yes 10 No 0
The image might not initially appear in the correct orientation. Using the orthoslice planes, how easy is it to rotate the image into the correct orientation?	easy ☐☐☐☐☐difficult 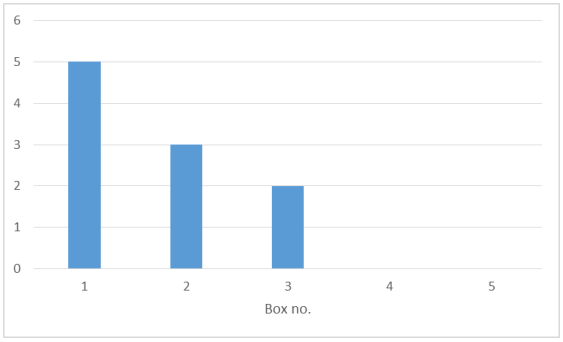

The “arbitrary slice” is a fourth slice which can be posed in any orientation

Disable the “x”, “y” and “z” slices and enable the arbitrary slice using the check boxes. Move the slice up and down using the “value” slider and rotate the slice using the two “normal” sliders.

Does the arbitrary slice appear correctly?	Yes 10 No 0
Do the interactive sliders move the slice as described above?	Yes 10 No 0
Does the slice remain within the bounds of the image box when it is moved?	Yes 10 No 0
How easy is it to move the diagonal slice to the position you want using the controls provided?	easy ☐☐☐☐☐difficult 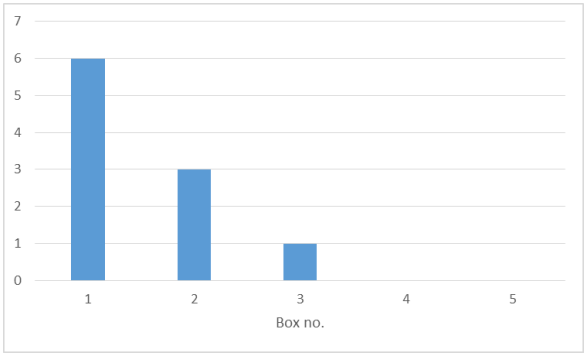

Tasks: View Image Volume

Select “View image volume” from the “Tasks” menu. This will display a medical image as a 3D volume rendering.

Does the image display as a semi-transparent coloured block?	Yes 8 No 2
Can you change the opacity using the “opacity” slider?	Yes 8 No 0
Using the range sliders, can you remove the background from the image, leaving just the torso and the arms?	Yes 8 No 0
How easy is it to set the sliders such that most of the image is removed but the kidneys are clearly visible?	easy ☐☐☐☐☐difficult 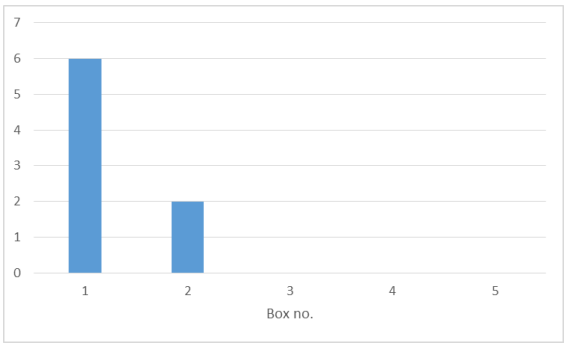

Tasks: View Image Pair 2D

An "image pair" is a medical image and its segmentation: that is, a labelling or annotation of the image indicating the voxels of interest.

Select "View image pair 2D" from the "Tasks" menu. Select the nephroblastoma dataset 5XIHQ from the selection dialog. This will display a medical image and its segmentation as a 2D slice. A kidney tumour is shown as a coloured overlay.

Does the image display as described?	Yes	10	No	0
Is the image in the correct orientation?	Yes	10	No	0
Using the check box on the "labels" control, can you switch the coloured overlay on and off?	Yes	10	No	0
Can you change the colour and transparency of the overlay?	Yes	10	No	0
Is the overlay positioned correctly on the tumour?	Yes	10	No	0
Can you read the total tumour volume from the right hand panel?	Yes	10	No	0

Tasks: View Image Pair 3D (nephroblastoma)

Select "View image pair 3D" from the "Tasks" menu. Select the nephroblastoma dataset 5XIHQ from the selection dialog. This will display a medical image and its segmentation as a 3D slice. A kidney tumour is shown as an isosurface (3D mesh object).

Does the image display as described?	Yes	10	No	0
Using the check box on the "labels" control, can you switch the isosurface on and off?	Yes	10	No	0
Can you change the colour and transparency of the tumour?	Yes	10	No	0
Is the isosurface mesh positioned correctly on the tumour?	Yes	10	No	0

Tasks: View Image Pair 3D (glioblastoma)

Select "View image pair 3D" from the "Tasks" menu. Select the glioblastoma dataset (ChicSeriesJun2015) from the selection dialog. This will display a brain image and its segmentation as a 3D slice. A tumour is shown as a set of coloured isosurfaces.

Does the image display as described?	Yes 10 No 0
Does the label control panel show four coloured labels?	Yes 10 No 0
Are the labels in the label control panel correctly named? (necrosis, oedema, non-enhancing and enhancing)	Yes 10 No 0
When more than one surface is displayed, does the transparency look natural and free from artefacts? (it might be necessary to first reduce the opacity of the surfaces using the sliders in the control panel)	Yes 10 No 0
With all surfaces selected, does the visualization respond quickly when the image is rotated?	very slow ☐☐☐☐☐very fast 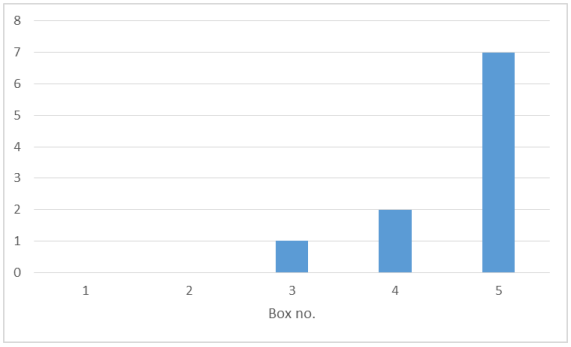

Tasks: View Image Pair Volume

Select “View image pair volume” from the “Tasks” menu. Select the nephroblastoma dataset 5XIHQ from the selection dialog. This will display a medical image and its segmentation as a volume rendering. The tumour segmentation is shown as an isosurface mesh within the volume rendering. The interaction is the same as in (6). Use the sliders to reveal the tumour isosurface.

Does the image display as described?	Yes 8 No 0
Does the visualization give a useful qualitative sense of the size and position of the tumour in the body?	not useful ☐☐☐☐☐very useful 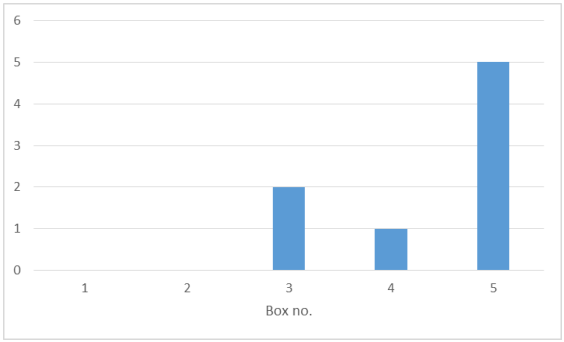

Using the check box on the “labels” control, switch the isosurface off.

How easy is it to set the sliders such that most of the image is removed, leaving the tumour and kidneys visible?	easy ☐☐☐☐☐difficult 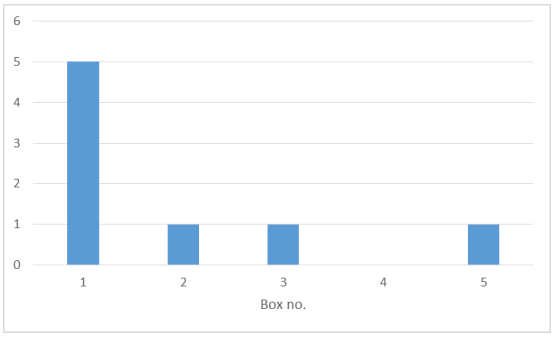

Tasks: View Image Pair Series (nephroblastoma)

Select "View image pair series 3D" from the "Tasks" menu. Select the nephroblastoma 5X1HQ dataset from the selection dialog. This will display a 3D slice visualization for an image series. This example shows a series containing two images: the pre-treatment image 0 and the post-treatment image 1.

Do the radio buttons in the "clinical image selection" panel successfully switch the image and tumour between image 0 and image 1?	Yes 10 No 0
Is the tumour clearly visible?	Yes 10 No 0
Is the tumour correctly placed in both images?	Yes 10 No 0
Does the "total tumour volume" update when the image changes?	Yes 9 No 0
Is this visualization useful in showing qualitatively how the tumour has changed as a result of treatment?	not useful ☐☐☐☐☐very useful 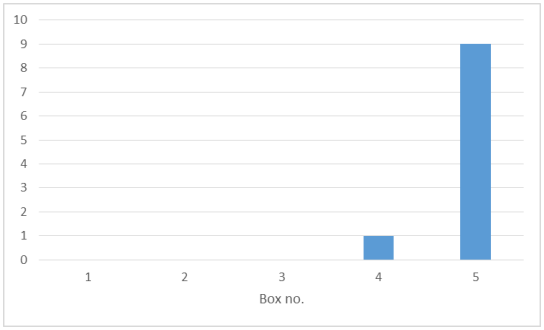

Tasks: View Image Pair Series (lung cancer)

Select "View image pair series 3D" from the "Tasks" menu. Select the lung dataset (LungSeries354) from the selection dialog. This will display a 3D slice visualization for an image series. This example shows a series containing two images: the pre-treatment image 0 and the post-treatment image 1.

Are the tumours clearly visible?	Yes 10 No 0
Are the tumours correctly placed in both images?	Yes 10 No 0
Is this visualization useful in showing qualitatively how the tumour has changed as a result of treatment?	not useful ☐☐☐☐☐very useful 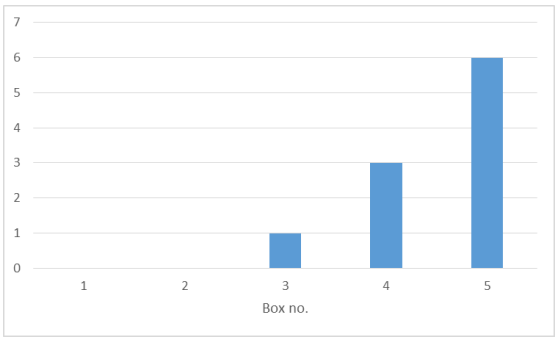

Tasks: View Simulation Series

Select "View CHIC sim series" from the "Tasks" menu. This will display a 3D isosurface visualization of a tumour simulation as a time series.

Does the simulated tumour display correctly?	Yes 10 No 0
Does moving the time slider show how the simulated tumour changes with time?	Yes 10 No 0
Does the visualization respond quickly when the time slider is moved?	very slow ☐☐☐☐☐very fast 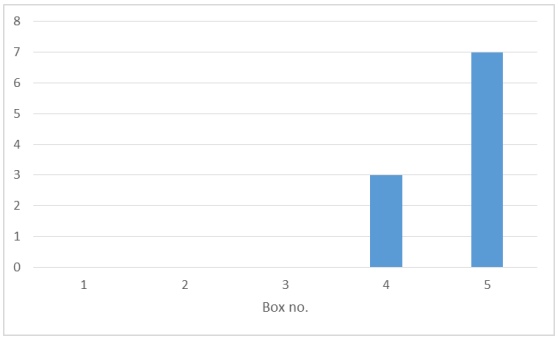

Open the "Plot View" tab to show a plot of the simulated tumour volume against time. The plot shows the result of four chemotherapy treatments, each resulting in a decrease in volume, followed by an upturn in the graph showing the start of regrowth. (The last shrinkage is quite small).

Does the plot correctly display the information as described?	Yes 10 No 0

Tasks: Compare parallel 2D

Select "Compare Mha/Sim parallel 2D" from the "Tasks" menu. Select the nephroblastoma series 5XIHQ. (The simulation will load automatically because it is the only dataset of this type). This will display two medical images side-by-side. The image on the left is the real clinical image and tumour. The image on the right is the clinical image with the simulated tumour. The real and simulated tumours are the same at the start, so the initial pair of images is identical.

Move the time slider to show how the simulated tumour changes with time. The slice control slider may need adjusting to keep the image slice positioned in the centre of the simulated tumour.

Does the time slider correctly show the tumour shrinking?	Yes 10 No 0

Select the radio button for image 1. The image on the left will change. (The image on the right does not because the simulation always takes place in the frame of image 0). Switch between image 0 and image 1 and back again. Image 1 should be registered – that is, it has been rotated and translated so that its coordinate system is as closely matched as possible to that of image 0.

When switching back and forth between image 0 and image 1, how closely matched are the positions of anatomical features in the two images?	poor ☐☐☐☐☐very good 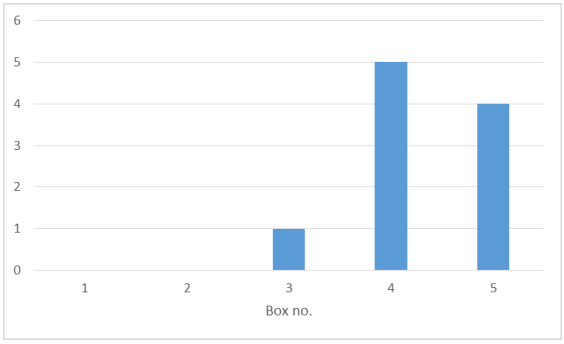

Move the time slider to the end of the simulation and select the radio button for image 1. This is now a comparison between the post-treatment (real) tumour on the left and the final simulation on the right. Adjust the z slice position if necessary to see the tumours.

Is the comparison useful in showing how well the simulation matches the real tumour in final position? (Please rate the usefulness of the comparison – not the accuracy of the simulation)	not useful ☐☐☐☐☐very useful 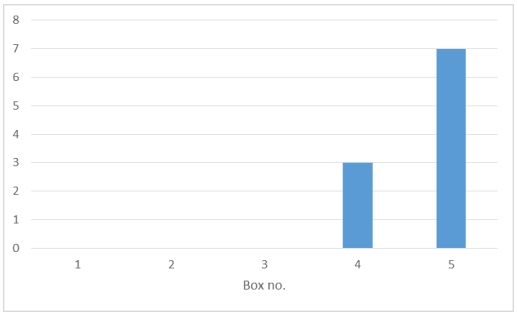
Is the comparison useful in showing how well the simulation matches the real tumour in final size?	not useful ☐☐☐☐☐very useful 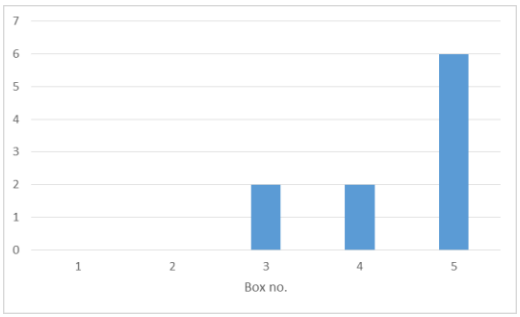

Select the "Plot View" tab. This shows a plot of the simulated tumour volume against time, with additional data points (red crosses) showing the volume of the real tumour before and after treatment.

Is the plot useful in showing how well the simulation matches the real tumour in final size?	not useful ☐☐☐☐☐very useful 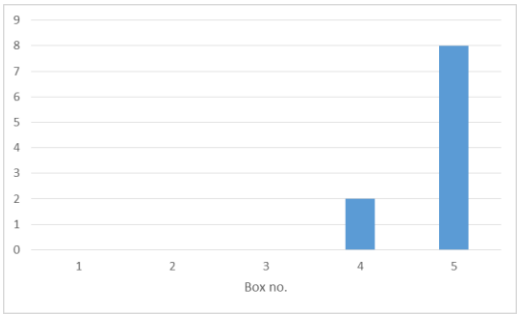

Tasks: Compare parallel 3D

Select "Compare Mha/Sim parallel 3D" from the "Tasks" menu. Select the 5XIHQ dataset. This shows a parallel 3D slice view, with the real image and tumour on the left and the simulated tumour on the right. Use the controls in the same way as the previous task to compare the final real and simulated tumours.

Is the comparison useful in showing how well the simulation matches the real tumour in final position? (Please rate the usefulness of the comparison – not the accuracy of the simulation)	not useful ☐☐☐☐☐very useful 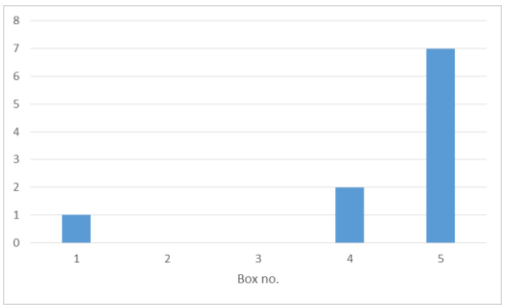
Is the comparison useful in showing how well the simulation matches the real tumour in final size?	not useful ☐☐☐☐☐very useful 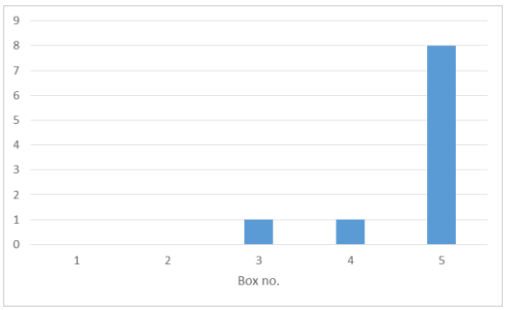

Tasks: Compare superimposed 3D

Select "Compare Mha/Sim superimposed 3D" from the "Tasks" menu. Select the 5XIHQ dataset. This shows a comparison between superimposed isosurfaces in the same 3D space. The "Comparison components" checkboxes at the top of the right hand panel select which isosurfaces are displayed in the view. The options are: real0 (the baseline real tumour at t=0), sim0 (the baseline simulated tumour at t=0), real(t) (the real tumour corresponding to the image selected by the radio buttons) and sim(t) (the simulation at the current position of the time slider).

Select sim(0) and sim(t) only, and move the time slider.

Is the comparison useful in showing how the simulated tumour changed in size and position relative to its starting state?	not useful ☐☐☐☐☐very useful 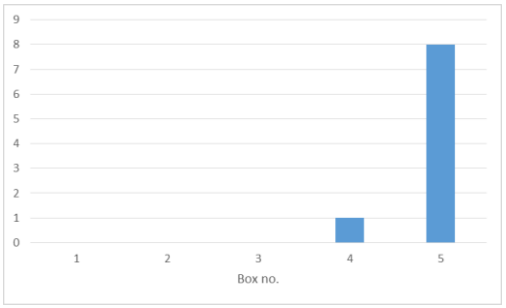

Select real(0) and real(t) only, and select the "Image 1" radio button.

Is the comparison useful in showing how the real tumour changed in size and position relative to its starting state?	not useful ☐☐☐☐☐very useful 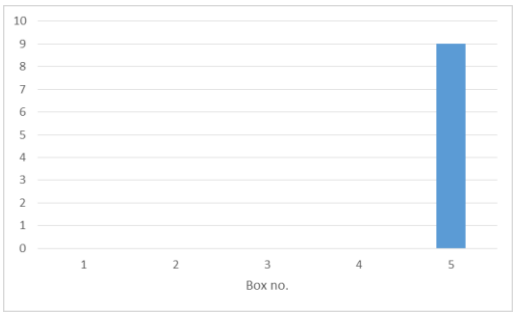

Select real(t) and sim(t) only, and select the “Image 1” radio button. Slide the time slider from t=0 to its final position.

Is the comparison useful in showing how well the simulation matches the real tumour in final position? (Please rate the usefulness of the comparison – not the accuracy of the simulation)	not useful ☐☐☐☐☐very useful 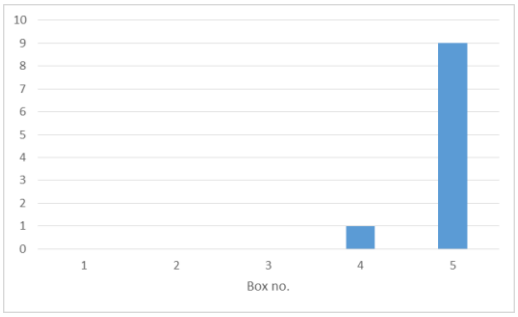
Is the comparison useful in showing how well the simulation matches the real tumour in final size?	not useful ☐☐☐☐☐very useful 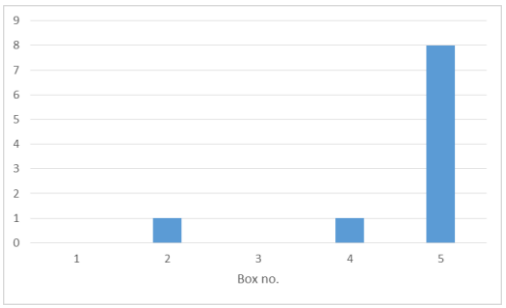

General

Is CCGVis easy to use?	difficult ☐☐☐☐☐very easy 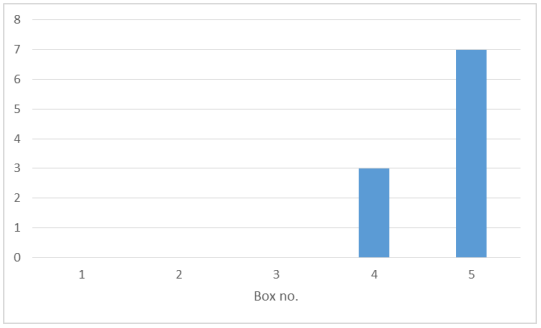
Are the interactions in CCGVis responsive?	very slow ☐☐☐☐☐very fast 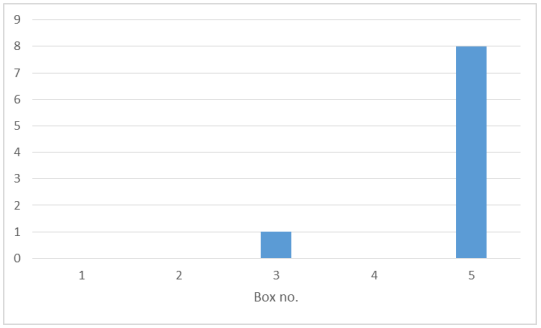
Is there always enough space on the screen for the control widgets?	Yes 10 No 0
Are the visualizations useful for comparing real and simulated tumours?	not useful ☐☐☐☐☐very useful 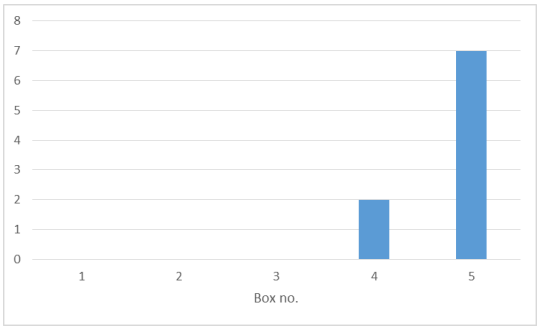

Conclusions and additional comments

- CCGVis launched successfully for all users.
- All CCGVis features worked for all users except for problems running the volume rendering on virtual machines (see below)
- CCGVis was rated as easy to use by all users.
- CCGVis was rated as having a fast response speed by all but one user.
- All users reported sufficient screen space for the control widgets, with the smallest screen size tested being 1280 x 800 on a small laptop.
- All user rated CCGVis as useful or very useful for comparing real and simulated tumours.
- Most users were able to use the volume rendering controls to perform a task without

significant difficulty.

- The 3D time series visualization was rated as useful for showing the change in the tumour. It appeared to be more useful in the nephroblastoma case than the lung cancer case, perhaps because of the small size of the lung tumours.
- The registration of images in a time series was qualitatively rated by users as good, and probably as good as can be achieved within the limits of rigid registration. Future improvement will require additional non-rigid registration.
- The comparison visualizations were rated good or very good by most users for comparing the tumour positions, and slightly less - adequate to very good - for comparing sizes. This is not surprising since the visualization does convey the quantitative information which is available from a number or a graph plot. The 3D superimposed comparison was rated the highest and the 3D parallel the least. Future development of CCGVis should ensure that the quantitative size of all compared tumours is displayed on the control panel.
- The two users running CCGVis with Windows emulators on MacOs were unable to view the volume rendering, because the virtual machines did not support the required OpenGL version. Future development of CCGVis should include a version cross-compiled for MacOs and Linux.
- One user became confused by accidentally using an experts-only feature in the control panel. Future versions of CCGVis should ensure that such features are disabled by default.
- Some users are confused when presented with the list of data, because they are not sure if they are expected to select a dataset or just view the list.
- One user with a small screen wished to be able to adjust the fraction of screen space given to the render window. However, this would difficult because it would conflict with the minimum size of the control widgets.
- Two users commented that the 2D image views should have a zoom function.
- One user suggested that the orthoslice view should be accompanied by 2D thumbnails of the image projections, each showing the transect of the slice. This would be particularly useful with the arbitrary slice.
- A nephroblastoma expert requested that tumour shape information should be displayed.
- One user suggested that each visualization should let the user have more instant access to similar visualizations with the same data.
- The 3D views, especially the simulation-only view, should contain coordinate axes.
- Some text information was requested:
    - Instructions for using the controls should be available.
    - Visualizations should be accompanied by some text information about what is being displayed.
    - Titles of images could be displayed underneath.
- A reset button for opacity in the volume rendering would be helpful.
- The 3D comparison currently has no image to give context to the simulation. There should be an orthoslice on both sides. Future development should reinstate the right-hand orthoslice, which was removed in early versions because of the need for two sets of

slice controls; this is no longer the case.

- In the superimposed comparison, the connection between selecting real(t) and the radio button “Image 1” is not obvious. Instructions would help.

2.7 Conclusions and Outlook

CCGVis is a useful tool for the visualization and comparison of tumours. It can accept medical images and their segmentations in a variety of formats, and compare them with simulations of tumour growth. Data can be viewed as 2D, 3D and volume rendering visualizations, as well as statistical plots.

CCGVis is well-documented with a flexible modular architecture, making it easy to add new visualizations and features.

CCGVis has been evaluated and found to be easy to use, fast and useful by its users.

CCGVis functions well on desktop PC’s and small laptops.

CCGVis includes the 3rd party library ITK, which has been used in a minor thresholding task to demonstrate that image processing can be performed in the CCGVis framework. Future versions may include image segmentation algorithms such as that described in Section 3 of this report.

Future versions of CCGVis will improve the interface according to suggestions in the evaluation exercise. The most important of these are: to cross-compile a version for MacOs; to improve the registration with a non-rigid algorithm; to add zoom functionality to the 2D views; to add more text annotations and instructions; and to add more quantitative data to the display.

CCGVis

3 Nephroblastoma image segmentation

Nephroblastoma or Wilms' tumour is a form of kidney cancer that affects around 80-85 children in the UK each year (Macmillan Cancer Support, 2016). Nephroblastoma generally affects children below the age of five and it may begin to develop in the womb when the baby is still unborn. The most common symptom is a painless swelling in the abdomen. Nephroblastoma rarely affects adults. In most cases it affects only one kidney (unilateral), but it can also affect both (bilateral). Nephroblastoma is a fast growing tumour with a median tumour size of around 400 ml at the time of diagnosis. Fortunately due to prospective clinical trials and effective treatments more than 90% of patients can be cured today. Imaging analysis tools play an important role in diagnosis and treatment planning. The assessment of the tumour during preoperative chemotherapy is of prognostic relevance and is crucial for postoperative treatment stratification (David *et al*., 2012).

Over the past years, many segmentation methods of different types of tumours such as glioblastoma, prostate and Wilms') have been proposed (Gordillo *et al*., 2013; Pham *et al*., 2000). These methods include full automated and semi-automated methods and they are applied to interpret scans such as MRI, CT or ultrasound. Each technique has its own advantages and disadvantages. Many of these methods fail due to different acquisition conditions of resolution, illumination and field of view, and the variability of body shapes and positions. Overlapping tissue and organs and the irregular size of the tumours can also cause a significant degradation to the performance of the segmentation methods, particularly the fully-automated methods.

For the above reasons, there is a need for reliable and robust semi-automated segmentation methods for Wilms' tumour studies. Semi-automated tumour segmentation techniques are computational methods that perform an extraction of the tumour tissue from multi-sequence Magnetic Resonance Imaging (MRI) with the interaction of human experts. These methods can provide important time-saving for neuro-radiologists in tumour assessment, and their accuracy can enhance tumour characterisation for radiotherapy, surgical planning and drug development assessment.

The aim of this document is to report findings during the CHIC project for semi-automated Nephroblastoma tumour segmentation in multi-sequence MRI imaging. In the following section, we briefly review some previously-proposed tumour segmentation methods.

3.1 State of the art in tumour image segmentation

Image segmentation aims to partition an image into sub-regions. These regions can be classified according to the functional areas, tissue types, structures of interest etc. (Bauer *et al*., 2013). The segmentation of Wilms' tumour is not a trivial task due the complexity, inhomogeneity and variability of its structures (Farmaki *et al*., 2010) and may require inputs such as seed-points, location and shapes from human experts. For this reason, a fully automated segmentation method may not be a good option for clinical use (David *et al*., 2012; Farmaki *et al*., 2010). Thus, a semi-automatic tumour segmentation method can be a good alternative option for Wilms' tumour analysis in multi-sequence MRI scans.

The semi-automated tumour segmentation methods can be divided into three major groups (Farmaki *et al*., 2010): region-based approaches, deformable model-based approaches and graph-based approaches.

The region-based approaches perform the tumour segmentation using a single seed point and expand the pixel extraction from that seed point to fill a defined coherent region according to a similarity measure of neighbouring pixels within the image region (Adams & Bischof, 1994). The region-based approaches include region-growing and watershed methods. A typical region-growing approach was proposed in Kim & Park (2004). This combined the region-growing algorithm with a texture-based analysis operation, which was performed on sample images of the tumour to define a

seed region as a starting point of the region-growing algorithm. Mancas & Gosselin (2003) proposed a semi-automatic segmentation on head and neck tumours in CT, MRI and PET scans. The approach used a marker-based watershed technique, by incorporating a fuzzy region with a tumour probability from 0 to 1. The watershed algorithm was used iteratively. This combination improved the watershed algorithm and avoided the over-segmentation problem.

The region-based methods have specific advantages over other segmentation approaches: they are easy to implement and produce coherent regions. However they often perform poorly because they cannot find objects that span several disconnected areas, and decisions regarding region membership can be difficult.

The deformable model-based approaches such as active contours (snakes), level sets (LS), or geodesic active contours have been extensively used in medical image segmentation applications. They make use of regional properties or edge detection in the image to extract the tumour regions (Bauer *et al*., 2013; McInerney & Terzopoulos, 1996). Methods such as level-set evolve toward the tumour region by searching in the image the largest gradient or by using region characteristics in the image. Wang *et al*. (2009) proposed a fluid vector flow algorithm to evolve a contour toward the boundary of the tumour in T1-weighted images. Linguraru *et al*. (2009) presented a semi-automated renal tumour quantification and classification method in a 3D size volume. The model combined a fast-marching operation and geodesic level-sets to define the shape of the lesions. Sachdeva *et al.* (2012) used a content-based active contour (CBAC) texture and intensity information to evolve an active contour toward the tumour boundary edge in MRI scans. Gu *et al*. (2006) proposed a multistage method for a 3D segmentation of CT and MRI images and a new radial distance-based segmentation validation approach. Gu's algorithm is based on level sets and it incorporates an improved fast marching method and a morphological reconstruction model.

Although deformable model-based approaches give very promising results, their implementations are more complicated than that of both region-based and graph bases approaches. They can also suffer from a high computational cost, intensity variation and image artefacts. Their segmentations often fail on heterogeneous objects when they are used in their traditional form, due to local minima.

The majority of deformable model-based methods use prior knowledge of the tumour tissues (i.e. intensities, shapes, colour, texture, positions etc.) to apply constraints on the segmentation algorithms. These constraints can lead to segmentation errors when the algorithms are used on different image modalities (Kaba *et al*., 2015).

The graph-based approach is one of the most attractive segmentation methods in Computer-aided diagnosis (CAD). Like the deformable model-based approaches, the graph-based image segmentations are also based on energy optimisation. They combine boundary regularisation with regularisation of regional proprieties in the same approach as Mumford-Shah (Boykov & Funka-Lea, 2006). The segmentation is performed by dividing the image into sub-classes known as Foreground (targeted tumour) and Background.

The segmentation process is performed using a graph, which consists of a set of nodes (i.e. pixels) and a set of edges (i.e. weights on the nodes) that connect the nodes using their degrees of similarity (intensity). A 3D semi-automated graph cut-based segmentation algorithm of liver cancer is proposed in Esneault *et al*. (2007). The liver cancer in a contrast-enhanced 3D CT volume was segmented with a user interaction in the selection of initial seeds for the foreground or background. These seeds are then used as a training base for the final segmentation of cancer tissue. Kaba *et al*., (2015) proposed the segmentation of retinal layer boundaries using graph cuts and continuous max-flow in optic coherence tomography scan (OCT).

The segmentation algorithm incorporated a kernel-induced space and a continuous multiplier-based max-flow algorithm to perform the segmentation of different retinal layers.

The graph-based segmentation methods are very powerful techniques because they allow the incorporation of prior knowledge (shapes, positions, sizes, seeds, textures) into the graph energy formulation to guide the algorithm defining the optimal segmentation results (Salazar-Gonzalez *et al*., 2014). Although the graph-based approaches produce good segmentation results, their performances often depend on the selection of initial seed points as well as the parameters search (Farmaki *et al*., 2010). The graph algorithm may also have problems in finding the appropriate cost functions of the graph functional to distinguish individual tumour tissue.

An automated segmentation of the nephroblastoma tumour is not trivial. To produce an acceptable segmentation results, the segmentation algorithm will rely heavily on the prior knowledge such as shape, colour, texture, positon. Therefore, a semi-automated segmentation method appears to be the best choice for the analysis of nephroblastoma scans in the clinical domain. This allows the interaction of expert physicians in order to guide the segmentation algorithm.

Our method serves this purpose, it allows the radiologists to interact with a 2D image slice. This slice includes all the multi-sequence MRI from which they can select tumour seed-points in one of the many slices and perform a full segmentation of the nephroblastoma tissue. The proposed method could eliminate the need of manual annotation of nephroblastoma and it can be used for high-throughput studies, such as clinical trials.

The rest of the paper is organized as follows. Our segmentation method is discussed in Section 3.2. Section 3.3 shows the evaluation results of the proposed method and conclusions are presented in Section 3.4.

3.2 Tumour Extraction

In this study, a semi-automatic segmentation of nephroblastoma in multi-sequence MRI scans is performed. The first step of the segmentation algorithm consists of removing some common artefacts of MRI medical imaging from the scans (i.e. noise, intensity inhomogeneity). This pre-processing operation is performed using a bias correction algorithm (Tustison *et al*., 2010). The tumour extraction in multi-sequence MRI scans is performed by adapting a continuous max-flow min-cut approach (Yuan et al., 2010). This includes a free 2D hand drawing tool, which allows human experts to select a region of interest (i.e. tumour seeds) and a kernel-induced segmentation functional (Salah et al., 2011). Figure 3-1 shows the illustration of the proposed method.

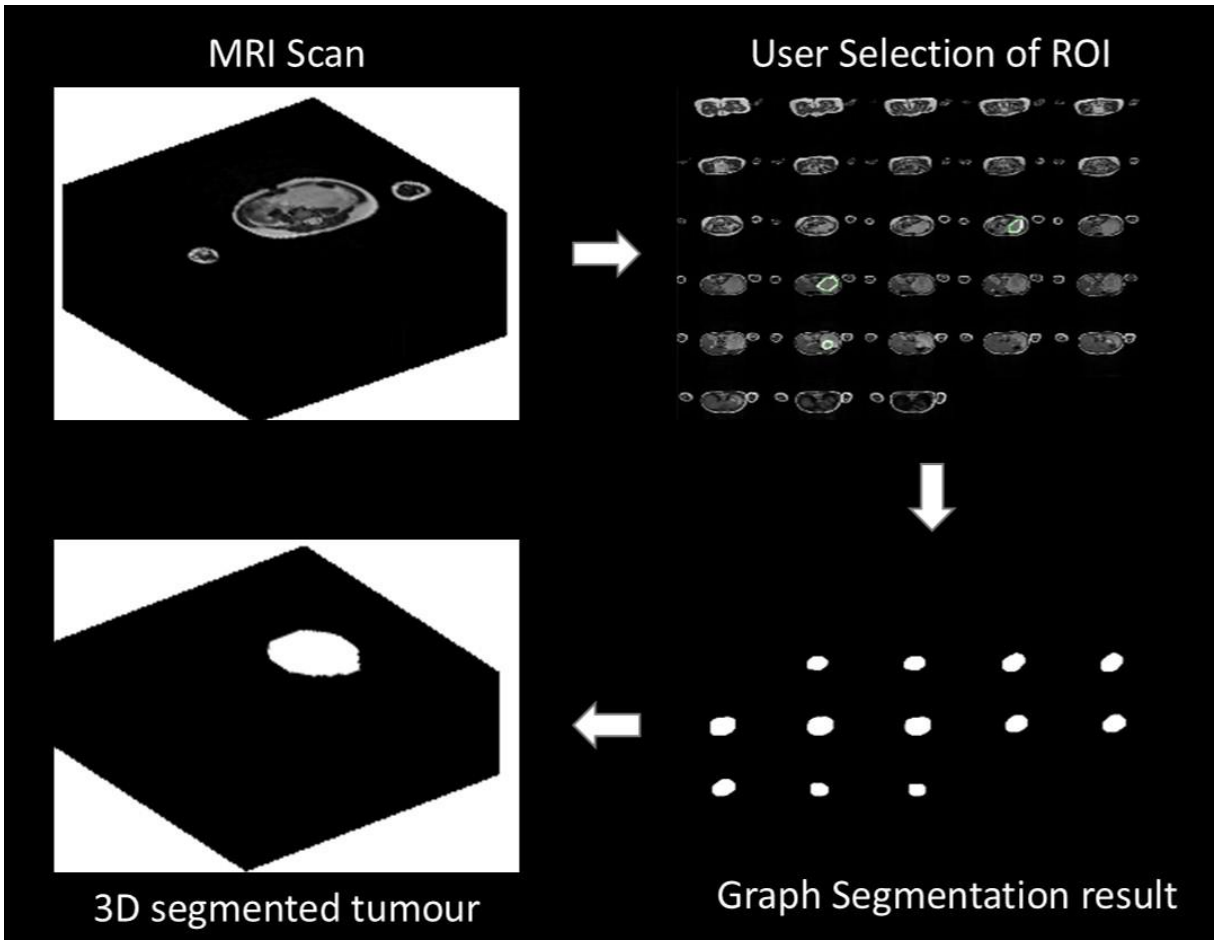

Figure 3-1 Illustration of different processes of the method. Top left: 3D MRI image. Top right: 2D slice for expert user selection of tumour seeds. Bottom left right: segmentation results of 2D slice. Bottom right: segmentation result 3D MRI.

Generally, the fuzziness of tumour boundary (lack of clear edges) in multi-sequence MRI scans is caused by the presence of imaging artefacts such as noise, inhomogeneity and similarity to surrounding tissues. The bias correction operation (Tustison *et al*., 2010) is used to correct these issues in the images to allow a correct segmentation of the tumour. The operation is performed by estimating the residual bias field. This residual is then subtracted from the corrupted scans to enhance the tumour. The bias correction operation can also reduce false positives during the segmentation process.

To perform the segmentation of nephroblastoma tumour from multi-sequence MRI scans, we represent each pixel point in a scan as a graph $G(\vartheta, \epsilon)$ consisting of a set nodes ϑ (i.e. pixels) and a set of edges ϵ connecting neighbouring nodes or pixels $\{p, q\}$. The nodes also include two special nodes known as terminals S (foreground: $tumour\ seeds$) and T (background $seeds$). Each pair of neighbouring pixels $\{p, q\}$ in the image grid is connected by n-links (i.e. edge between pixels). Each pixel p is also connected foreground terminal and background terminal through t-links. All edges in the graph including both n-links and t-links are assigned some positive weights based on the similarity measured between pixels (i.e. intensities). After creating the graph, the segmentation is performed by producing a cut through the graph. The preferred cut or path will have the minimum total weights of edges for travelling from a start node to an end node. The selected cut separates the MRI scan into two disjoint regions, one representing the tumour tissue (foreground) and the other one the rest of the image (background) as shown in Figure 3-2.

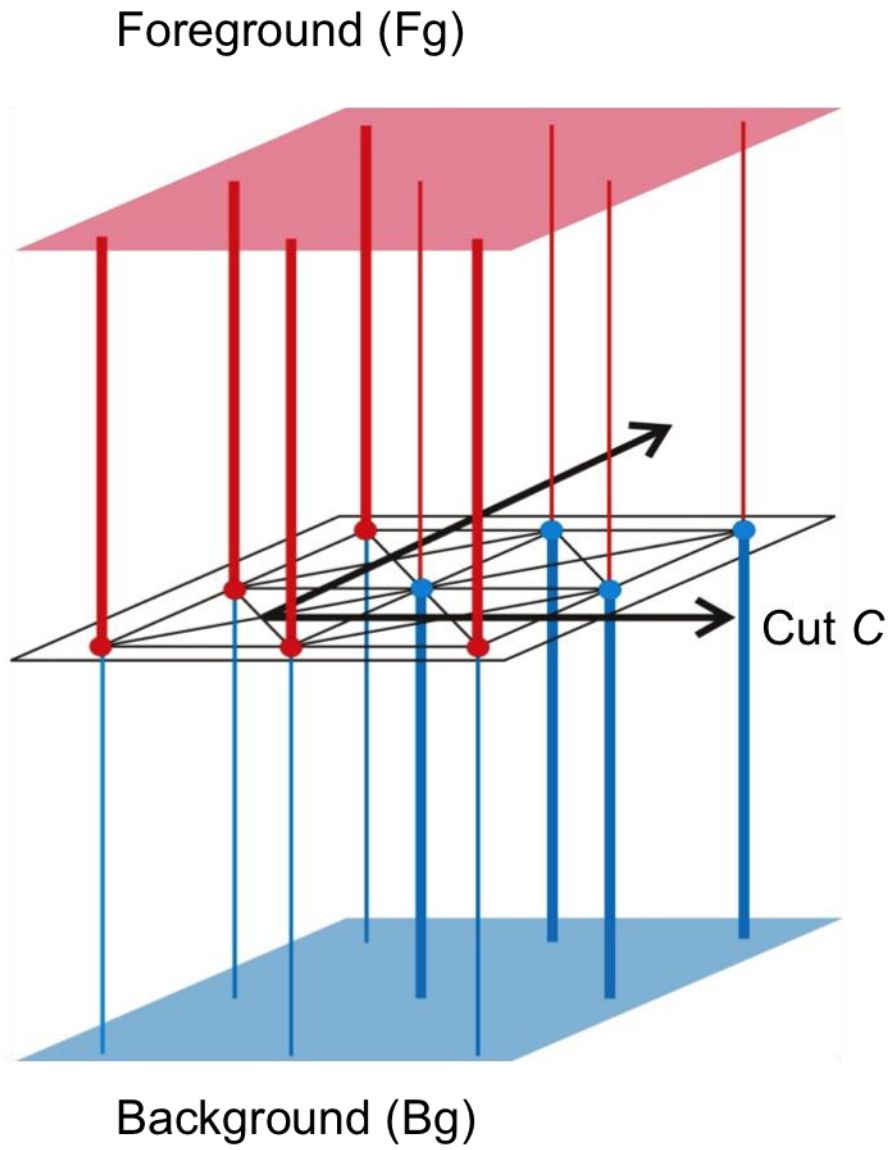

Figure 3-2 Graph construction. The red and blue dots represent the pixels in the image grid. The red and blue planes represent the labels of foreground and background to which the pixels are to be assigned. The thickness of the red and blue lines represents the strength of the link between the pixels and the labelled seed points.

The interactive segmentation is performed as follows: The slices in a scan are displayed as a single image object as shown in Figure 3-3. This operation allows the user to visualize all the slices that contain the tumour. The expert user can select a tumour seed region in one of the tumour slices (the red outlined area in Figure 3-3(a)), and the rest of the slices are automatically segmented by the proposed method, as shown in Figure 3-3(b). A set of images manually labelled by experts is shown in Figure 3-3(c). One of the advantages of this interactive segmentation is that it allows radiologists to interactively select tumour tissue in one of the scan slices to allow a complete extraction of the tumour and to avoid the segmentation of health tissues or other tissues similar to the tumour. It is also allows a global optimal solution for a graph segmentation, which is not possible in a fully automated segmentation methods.

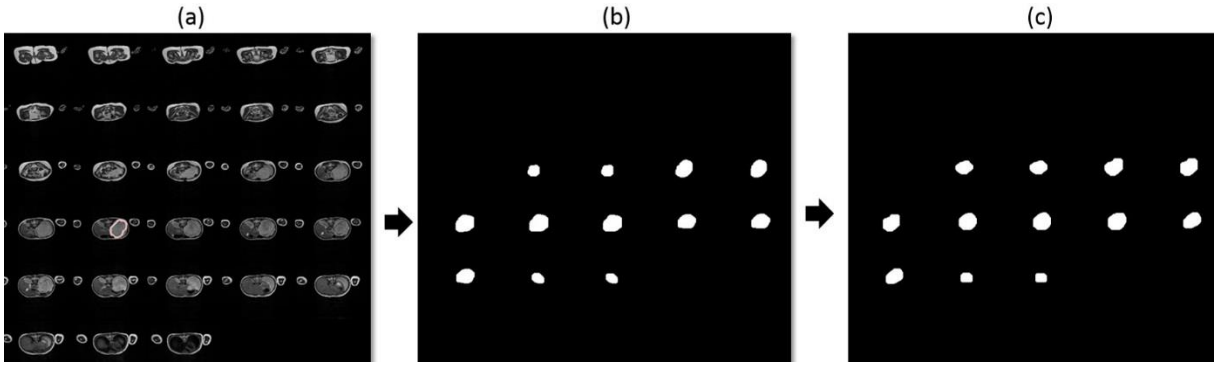

Figure 3-3 User section of tumour seeds. (a) The user select an ROI (tumour seeds) in red circle in one of the image slices. (b) The segmentation results of the methods in all the slices. (c) Images manually-labelled by experts.

3.3 Evaluation of the Segmentation Method

The multi-sequence MRI scan data used in this study was obtained from ongoing pioneering research conducted on Wilms' tumour in the department of Paediatric Oncology and Haematology at Saarland University Medical Centre in Homburg, Germany. The data set contains T2 weighted multi-sequence MRI scans with transversal cut of 24 cancer patients. Each patient has two scans, one before radio-chemotherapy and the other one after the radio-chemotherapy to determine the effectiveness of the treatment. In total we have 48 scans from the 24 patients. In addition to the data set, each scan was manually annotated by expert clinicians. Our method uses these expert hand-labelled tumours as a performance reference (Ground truth). The acquisition parameters of multi-sequence MRI are set differently by the operators to allow a better visualisation of different scans. The proposed method is implemented on MATLAB R2011b and the computation time of our algorithm is less than 80 seconds for each multi-sequence MRI scan on a MAC OX X running at 2.66 GHz, with 4G of RAM memory.

To evaluate the accuracy of our method, we compared our results against the expert's manual annotations. The evaluation is performed using statistical metrics such as the sensitivity (true positive rate), the specificity (true negative rate), the false negative rate and the average accuracy rate are shown in Table 3-1. Others metrics including the Dice coefficient, the root-mean-error and the Jaccard index are also used for the validation of spatial tumour shape representation in Table 3-2.

Table 3-1 Performance evaluation of our segmentation algorithm on 48 multi-sequence MRI scans. Using sensitivity (TPR), specificity (TNR), false positive rate (FPR), false negative rate (FNR) and the accuracy (ACC) with their respective standard deviations and 95% confidence interval.

Metrics	Average	Standard Deviation	Confidence Interval
Sensitivity (TPR)	0.9452	0.0429	0.0077
Specificity (TNR)	0.9966	0.0039	0.0007
FPR	0.0034	0.0039	0.0007
FNR	0.0548	0.0429	0.0077
ACC	0.9959	0.0039	0.0007

Table 3-2 Performance evaluation of our segmentation algorithm on 48 multi-sequence MRI scans. Using dice coefficient, root-mean-square (RMSE), and Jaccard index with their respective standard deviations and 95% confidence interval.

Metrics	Average	Standard Deviation	Confidence Interval
Dice	0.9060	0.0549	0.0098
Jaccard	0.8326	0.0898	0.0161
RMSE	0.0481	0.0309	0.0055

For illustration, we performed the box plots of the Dice coefficient, RMSE, TNR and TPR for the evaluation of our method as shown in Figure 3-4.

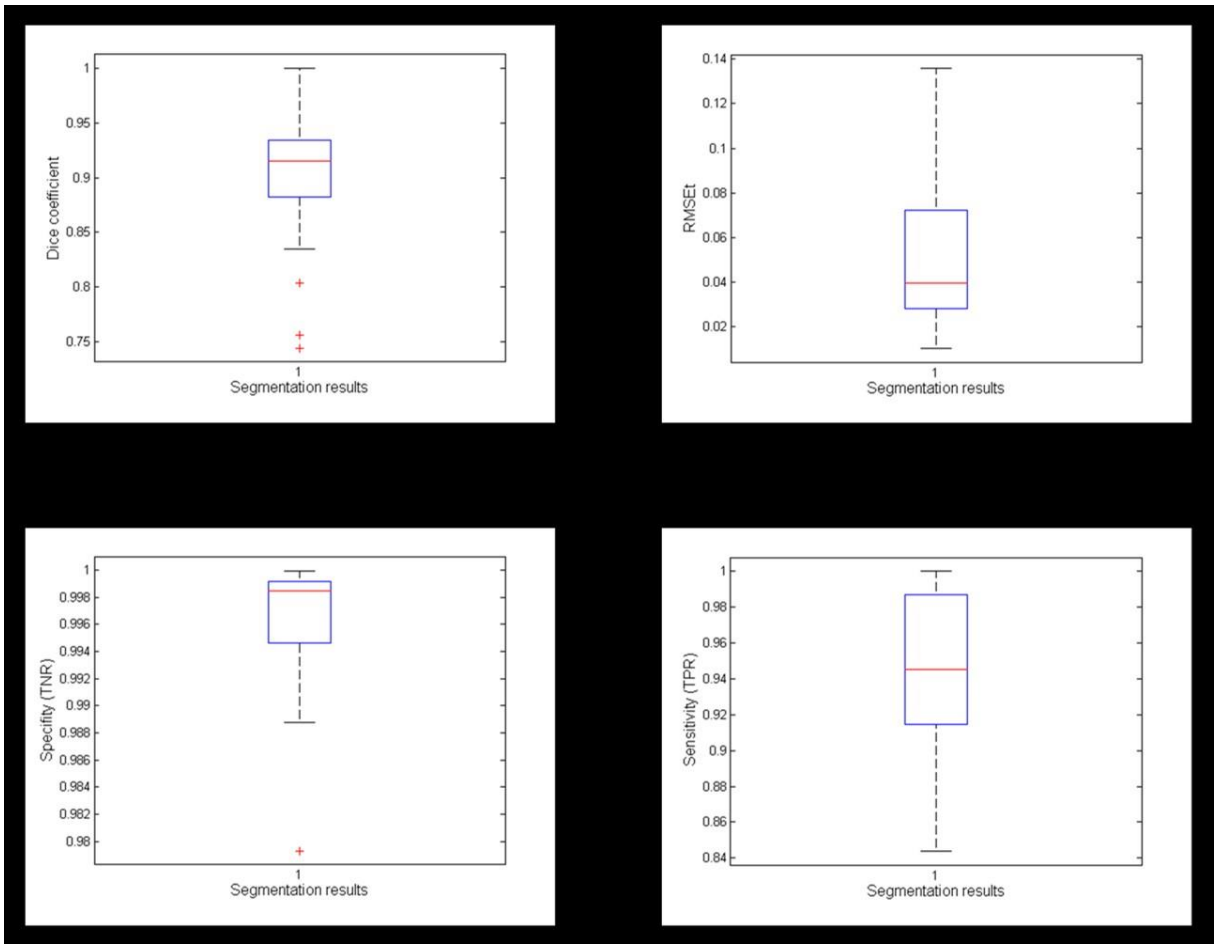

Figure 3-4 Box plots of Dice coefficient, RMSE, TNR and TPR of results evolution on the 48 MRI scans.

Figure 3-5 shows the segmentation results of a proposed method compared against experts hand labelled tumour. The segmentation of the tumour was also performed before and after the radio-chemotherapy as shown in Figure 3-6.

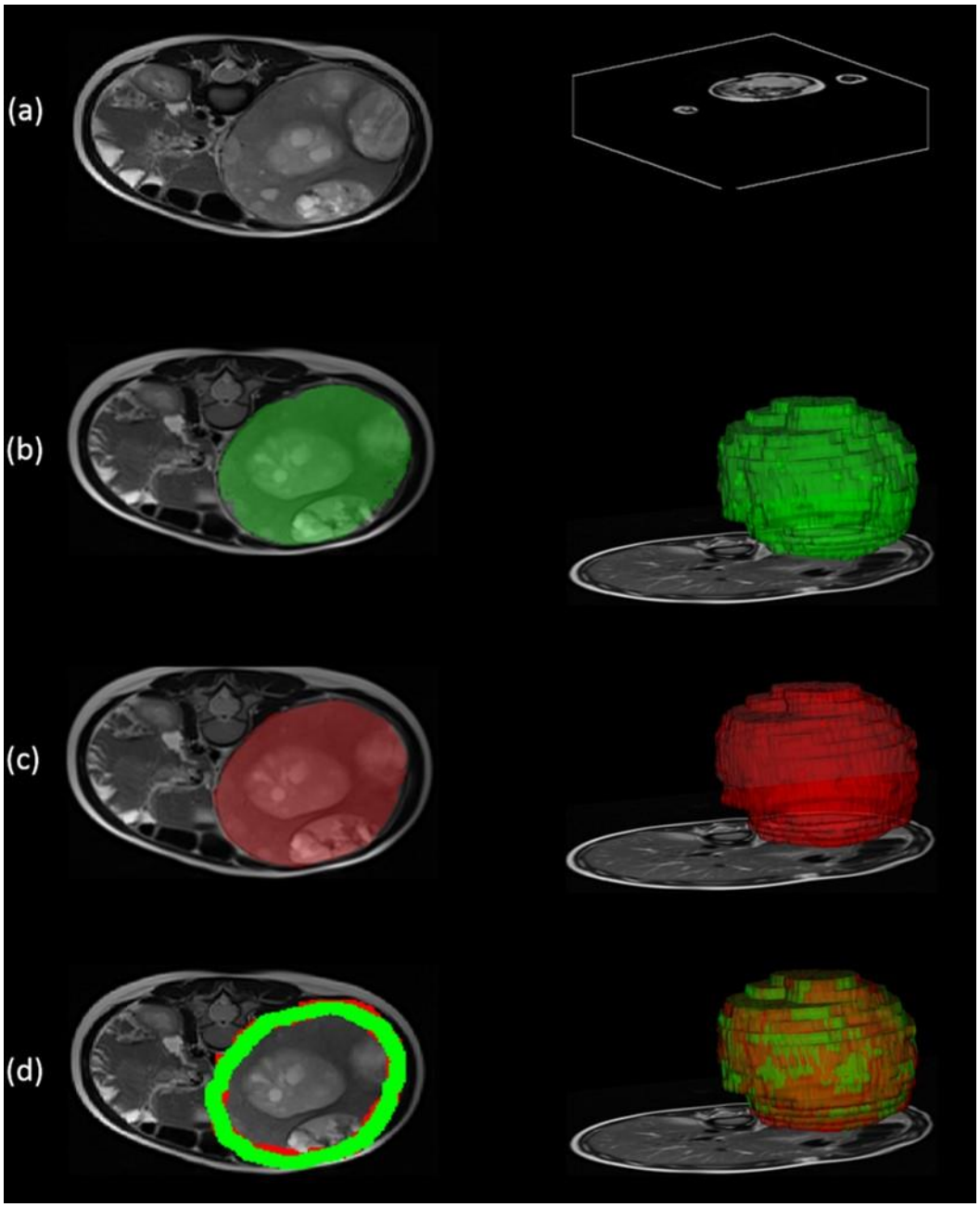

Figure 3-5 Segmentation results. Row (a): left 2D MRI image, right: 3D scan. Row (b): left segmentation result in 2D (in green), right: segmentation result in 3D (in green). Row (c): left experts hand labelled in 2D (in red), right: experts hand labelled in 3D (in red). Row (c): left overlap of the segmentation result and the experts hand labelled in 2D, right: overlap of the segmentation result and the experts hand labelled in 3D.

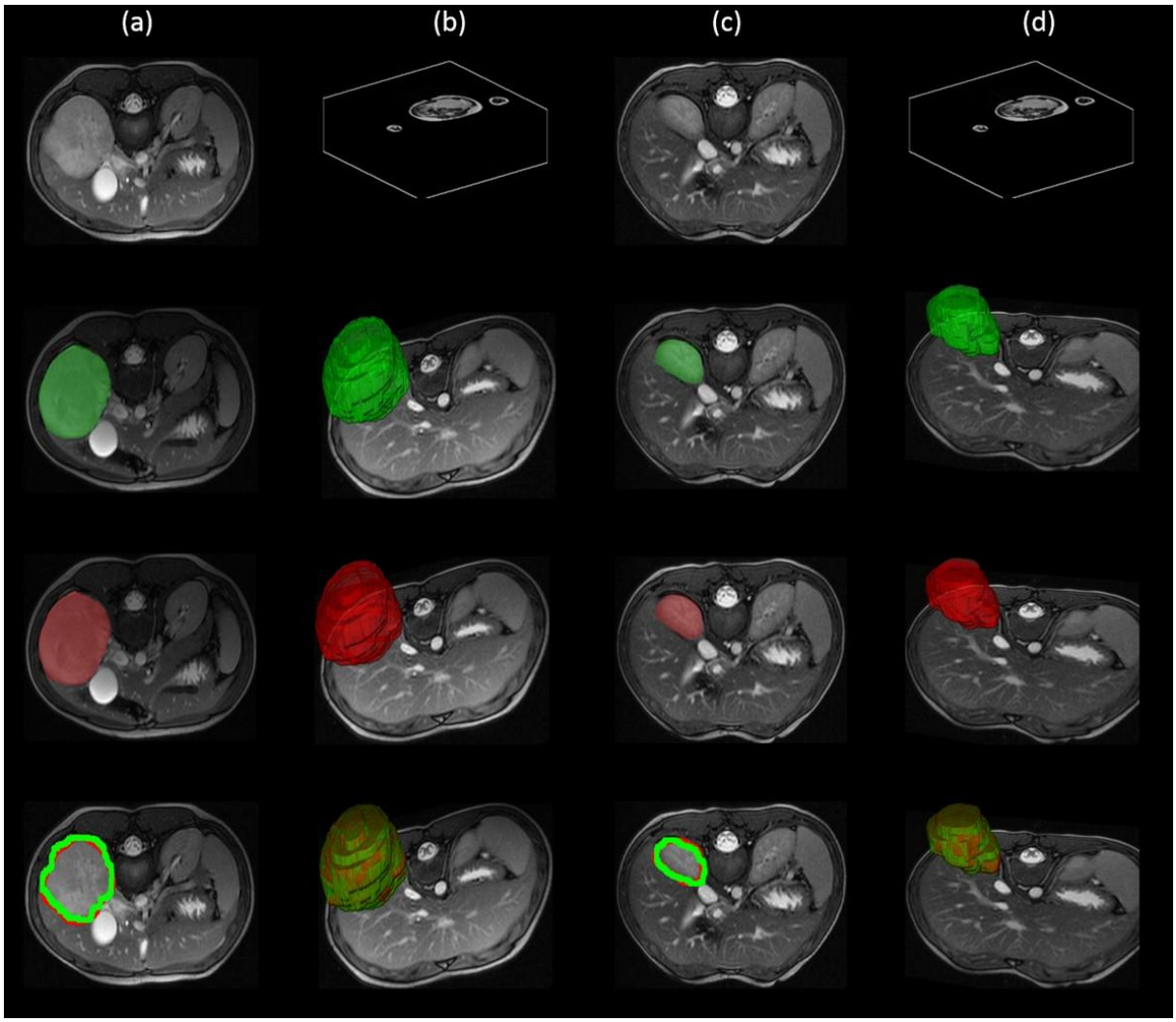

Figure 3-6 Segmentation results before and after radio-chemotherapy. Column (a): 2D MRI images, the segmentation results in green and in red experts hand labelled before therapy. Column (b): corresponding 3D images, the segmentation results green and in red experts hand labelled before therapy. Column (c): 2D MRI images, the segmentation results in green and in red experts hand labelled after therapy. Column (c): corresponding 3D images, the segmentation result green and in red experts hand labelled after therapy.

3.4 Conclusions and Outlook

In summary, we have developed a semi-automated method to extract Wilms' tumour from multi-sequence MRI scans. The method has been designed, tested and validated in conjunction with medical experts, enabling its deployment and exploitation in the clinical setting.

The overall procedure includes a pre-processing step that enhances the contrast of the tumour in a multi-sequence scan using a bias correction operation, and a tumour extraction step that includes kernel mapping and continuous max-flow algorithm. The method was validated on 48 multi-sequence MRI scans and it is proved to be accurate, robust, flexible, and fast, leading to a successful extraction of the tumour tissue. Our method has the advantage over fully automated segmentation methods because it allows an easy interaction of the user with different slices and facilitates the segmentation of irregular tumour boundaries as well as enabling the radiologist to make decisions regarding tumour size and shape.

During the research, we have identified challenges and opportunities that constitute the basis for future improvement and utilisation of the technique. Accuracy, robustness and flexibility of the algorithm is crucial for the assessment of the tumour for surgical planning and post-surgical assessment. The proposed method has the advantage over fully automated segmentation methods because it allows an easy interaction of the user with different slices and facilitates the segmentation of irregular tumour boundaries as well as enabling the radiologist to make decisions regarding tumour size and shape.

Radiomics is an emerging field where both imaging and non-imaging information are combined for non-invasive imaging biomarkers that can be used for assessing tumour phenotyping, association to genetic biomarkers (radiogenomics) using machine learning methods. These advances in imaging allow to further improve the current response to tumour analysis criteria that currently rely on over-simplistic metrics of tumour size and disease progression. Combining these methods with advanced Radiomics, and using machine learning methodologies would refine and personalise the evaluation of patient imaging data.

4 Timeline Visualization

This section describes work done by BED on a timeline visualization for the CHIC medical database. The software is based on the JavaScript library D3.js. Figure 4-1 shows the typical appearance of this visualization. The database items are colour-coded by type, and arranged along a zoomable timeline for interactive inspection.

Figure 4-1 Timeline visualization of medical database

The timeline visualization includes the following features:

- Zoom-in & Zoom-out
- Drag left and right
- Clustering

- Colour codes for different type of clinical data
- Brief description of content
- Download selected data

The interactive zoom is operated by the mouse scroll wheel. It allows the user zoom out for an overview, or zoom in for more detail in a narrower time range, as shown in Figure 4-2. The timeline automatically adjusts the timescale to hours, days, months or years. It is also possible to manually set a start and end time for the range.

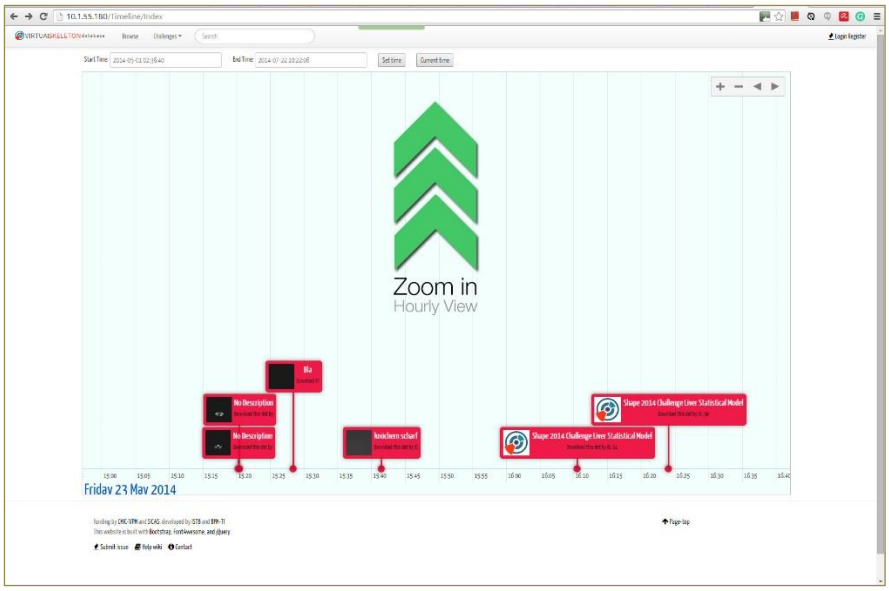

Figure 4-2 Effect of zoom on timeline, showing more detail in a narrower time range.

The user can also drag the timeline left and right to move along it, as shown in Figure 4-3.

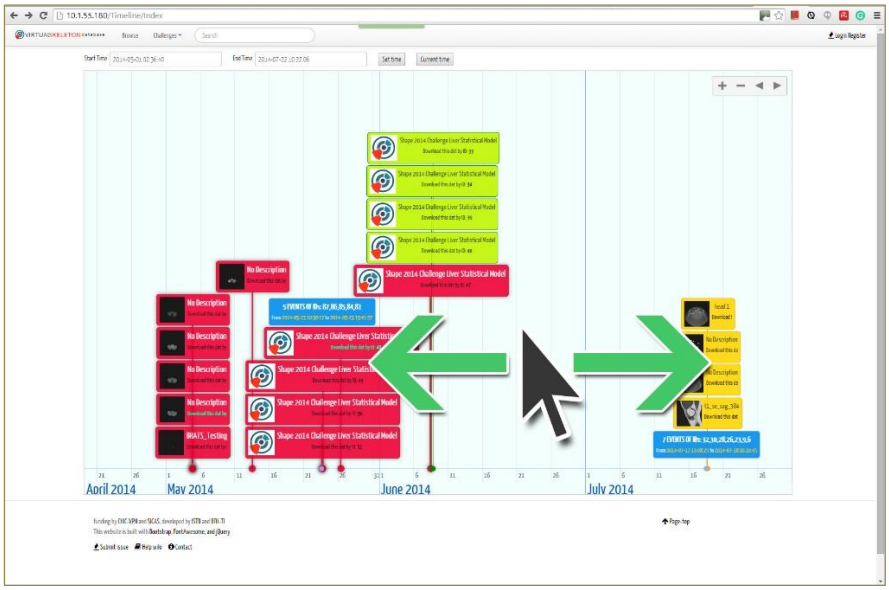

Figure 4-3 Effect of drag left-right, interactively moving along the timeline.

Clustering, shown in Figure 4-4, is used to group close-by items together to avoid clutter. In this example, the blue item represents a cluster of 3 items.

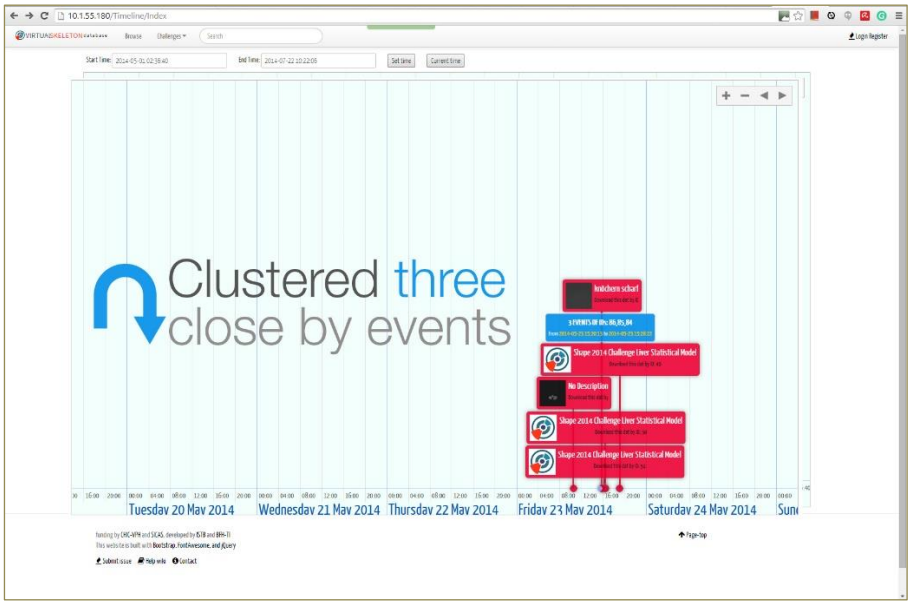

Figure 4-4 Clustering of close-by items to avoid clutter.

The items can be colour-coded by type, as shown in Figure 4-5.

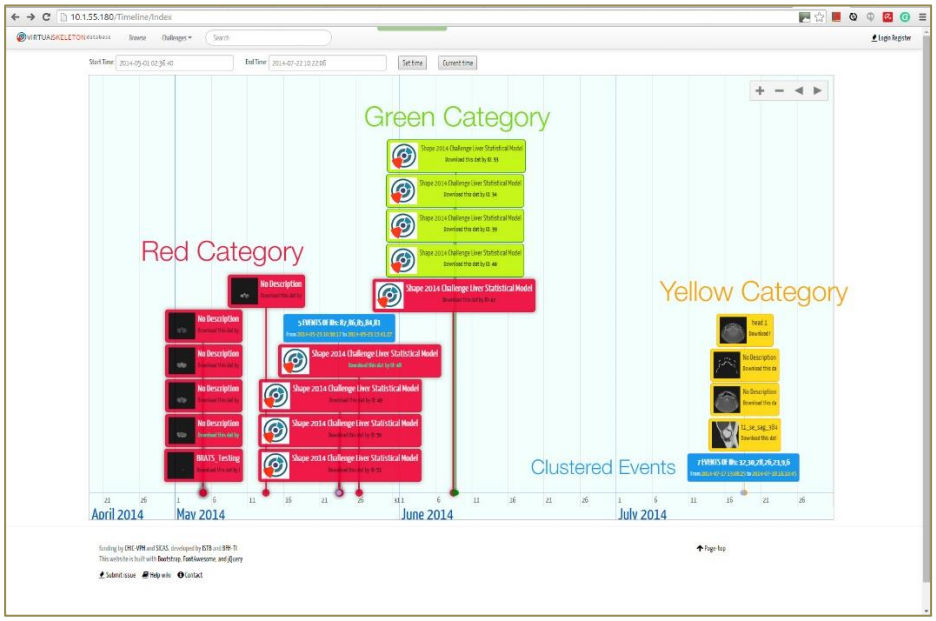

Figure 4-5 Colour coding of items.

The items can be annotated with brief content, including thumbnail images, as shown in Figure 4-6.

Figure 4-6 Content description, including thumbnail images.

The content description also features a hyperlink which can be used to directly download the item, as shown in Figure 4-7.

Figure 4-7 Content description showing download link.

5 References

Adams, R. & Bischof, L. (1994). Seeded region growing. *IEEE Transactions on Pattern Analysis and Machine Intelligence*, **16**(6):641–647. (doi: 10.1109/34.295913)

Bauer, S., Wiest, R., Nolte, L-P. & Reyes, M. (2013). A survey of MRI-based medical image analysis for brain tumor studies. *Physics in Medicine and Biology*, **58**(13):R97-129. (doi: 10.1088/0031-9155/58/13/R97)

Ben Salah, M., Mitiche, A., & Ben Ayed, I. (2011). Multiregion image segmentation by parametric kernel graph cuts. *IEEE Transactions on Image Processing*, **20**(2):545–557. (doi: 10.1109/TIP.2010.2066982)

Boykov, Y. & Funka-Lea, G. (2006). Graph Cuts and Efficient N-D Image Segmentation. *International Journal of Computer Vision*, **70**(2):109–131. (doi: 10.1007/s11263-006-7934-5)

CCGVis: a visualization tool for tumour comparison (2017) https://youtu.be/pR0USCxPwbM

David, R., Graf, N., Karatzanis, I., Stenzhorn, H., Manikis, G.C., Sakkalis, V., Stamatakos, G.S. & Marias, K. (2012). Clinical evaluation of DoctorEye platform in nephroblastoma. *Proceedings of the 2012 5th International Advanced Research Workshop on In Silico Oncology and Cancer Investigation - The TUMOR Project Workshop, IARWISOCI 2012*.

Dr Eye http://biomodeling.ics.forth.gr/?page_id=8

Esneault, S., Hraiech, N., Delabrousse, É. & Dillenseger, J.L. (2007). Graph cut liver segmentation for interstitial ultrasound therapy. *Annual International Conference of the IEEE Engineering in Medicine and Biology - Proceedings*, 5247–5250. (doi: 10.1109/IEMBS.2007.4353525)

Everitt, C. (2001) Interactive Order-Independent Transparency. NVIDIA Technical Report.

Farmaki, C., Marias, K., Sakkalis, V. & Graf, N. (2010). Spatially Adaptive Active Contours: A Semi-Automatic Tumor Segmentation Framework. *International Journal of Computer Assisted Radiology and Surgery*, **5**(4):369–384. (doi: 10.1007/s11548-010-0477-9)

Gordillo, N., Montseny, E. & Sobrevilla, P. (2013). State of the art survey on MRI brain tumor segmentation. *Magnetic Resonance Imaging*, **31**(8):1426–1438. (doi: 10.1016/j.mri.2013.05.002)

Gu, L., Xu, J. & Peters, T.M. (2006). Novel multistage three-dimensional medical image segmentation: methodology and validation. *IEEE Transactions on Information Technology in Biomedicine : A Publication of the IEEE Engineering in Medicine and Biology Society*, **10**(4):740–748. (doi: 10.1109/TITB.2006.875665)

Insight Segmentation and Registration Toolkit, ITK, www.itk.org

Kaba, D., Wang, Y., Wang, C., Liu, X., Zhu, H., Salazar-Gonzalez, A.G. & Li, Y. (2015). Retina layer segmentation using kernel graph cuts and continuous max-flow. *Optics Express*, **23**(6):7366–7384. (doi: 10.1364/OE.23.007366)

Kim, D-Y. & Park, J-W. (2004). Computer-Aided Detection of Kidney Tumor on Abdominal Computed Tomography Scans. *Acta Radiologica*, **45**(7):791–795. (doi: 10.1080/02841850410001312)

Linguraru, M.G., Yao, J., Gautam, R., Peterson, J., Li, Z., Linehan, W.M. & Summers, R.M. (2009). Renal Tumor Quantification and Classification in Contrast-Enhanced Abdominal CT. *Pattern Recognition*, **42**(6): 1149–1161. (doi: 10.1016/j.patcog.2008.09.018)

Lorensen, W.E. & Cline, H.E (1987). Marching cubes: a high resolution 3D surface construction algorithm. Computer Graphics **21**(3):163-169

Macmillan Cancer Support (2016). Wilms' tumor in children. https://www.macmillan.org.uk/cancerinformation/cancertypes/childrenscancers/typesofchildrenscancers/wilmstumour.aspx

Mancas, M. & Gosselin, B. (2003). Fuzzy tumor segmentation based on iterative watersheds. *Proc. of the 14th ProRISC Workshop on Circuits, Systems and Signal Processing (ProRISC 2003), Veldhoven (Netherland)*, 5. (doi: 10.1117/12.535017)

McInerney, T., & Terzopoulos, D. (1996). Deformable models in medical image analysis: a survey. *Medical Image Analysis*, **1**(2):91–108. (doi: 10.1016/S1361-8415(96)80007-7)

Multimod Application Framework, MAF, http://www.openmaf.org

Pham, D.L., Xu, C. & Prince, J.L. (2000). Current Methods in Medical Image Segmentation. *Annual Review of Biomedical Engineering*, **2**:315–337. (doi: 10.1146/annurev.bioeng.2.1.315)

Sachdeva, J., Kumar, V., Gupta, I., Khandelwal, N. & Ahuja, C.K. (2012). A novel content-based active contour model for brain tumor segmentation. *Magnetic Resonance Imaging*, **30**(5):694–715. (doi: 10.1016/j.mri.2012.01.006)

Salazar-Gonzalez, A., Kaba, D., Li, Y., & Liu, X. (2014). Segmentation of Blood Vessels and Optic Disc in Retinal Images. *IEEE Journal of Biomedical and Health Informatics*, 18(6):1874-1886. (doi: 10.1109/JBHI.2014.2302749)

Tustison, N.J., Avants, B.B., Cook, P.A., Zheng, Y., Egan, A., Yushkevich, P.A. & Gee, J.C. (2010). N4ITK: improved N3 bias correction. *IEEE Transactions on Medical Imaging*, **29**(6):1310–1320. (doi: 10.1109/TMI.2010.2046908)

Visualization Toolkit, VTK, www.vtk.org

Wang, T., Cheng, I. & Basu, A. (2009). Fluid vector flow and applications in brain tumor segmentation. *IEEE Transactions on Biomedical Engineering*, **56**(3):781–789. (doi: 10.1109/TBME.2009.2012423)

Yuan, J., Bae, E. & Tai, X-C. (2010). A study on continuous max-flow and min-cut approaches. *Proceedings of the IEEE Computer Society Conference on Computer Vision and Pattern Recognition*, 2217–2224. (doi: 10.1109/CVPR.2010.5539903)